Mutagenesis and structural modeling implicate RME-8 IWN domains as conformational control points

Anne Norris, Collin McManus, Simon Wang, Rachel Ying, Barth D. Grant

Abstract

After endocytosis, transmembrane cargo is differentially sorted into degradative or recycling pathways. This process is facilitated by recruitment into physically distinct degradative or recycling microdomains on the limiting membrane of individual endosomes. Endosomal sorting complexes required for transport (ESCRT) mark the degradative microdomain, while the recycling domain is marked by the retromer complex and associated proteins RME-8 and SNX-1. The separation of endosomal microdomains is also controlled by RME-8 and SNX-1, at least in part via removal of degradative component HRS/HGRS-1 from the recycling microdomain. This activity is likely due to recruitment and activation of chaperone Hsc70 to the recycling microdomain by the RME-8 DNAJ domain. To better understand the mechanism of RME-8 function we performed a new phylogenetic analysis of RME-8 and identified new conserved sequence features. In a complementary approach, we performed structure-function analysis that identified the C-terminus as important for microdomain localization and likely substrate binding, while N-terminal sequences beyond the known single N-terminal PH-like domain are important for endosome recruitment. Random mutagenesis identified IWN4, and by analogy IWN3, to be important for the inhibitory DNAJ domain binding. Combining AlphaFold structural predictions with *in vivo* truncation and point mutation analysis of RME-8, we propose a model whereby SNX-1 and the IWN domains control the conformation of RME-8 and hence the productive exposure of the DNAJ domain. Furthermore, we propose that the activation of RME-8 is cyclical, with SNX-1 acting as an activator and a target of RME-8 uncoating activity.

INTRODUCTION

First identified in our screen for Receptor Mediated Endocytosis (RME) mutants in *C. elegans* [1,2], RME-8 is a conserved endosomal regulator required for cargo sorting [3-9]. It functions with Sorting Nexin 1 (SNX-1) and the Retromer complex in endosome to Golgi recycling [9]. Together RME-8 and SNX-1 also negatively regulate the ESCRT complex that mediates degradation on the same endosomes [9,10] [11].

Endosome to Golgi sorting of transmembrane cargo occurs during the early to late endosome transition [12-14] (reviewed in [15]). Indeed, the recruitment of Retromer is dependent upon RAB-7, which is recruited to maturing endosomes during this transition [12]. The Retromer associated RME-8/SNX-1 marked recycling microdomain, and the ESCRT-0 marked degradative microdomain, are found adjacent to one another on endosomes during this transition [10]. The formation and separation of such endosomal microdomains are most easily studied in the context of *C. elegans* scavenger cells called coelomocytes, due to their naturally large endosomes that are typically more than 1 micron in diameter [10]. In this system we previously showed that RME-8 is required to preserve separation of recycling and degradative microdomains on sorting endosomes. In particular, RME-8 prevents overassembly of ESCRT-0 that encroaches on and mixes with recycling microdomains when RME-8 is missing [10,11]. This control of microdomains is a unique feature of RME-8 and SNX-1, as mutants lacking retromer components *vps-35* and *snx-3* have normal microdomain separation [10]. Like several other proteins involved in membrane trafficking, rare alleles of RME-8 have been implicated in neurodegenerative disorders such as Parkinson's Disease and Essential Tremor [16,17] (reviewed in [18-20]).

RME-8 is a large 260 kDa DNAJ domain protein with an N-terminal PI(3)P lipid binding domain and a C-terminal Retromer associated SNX-1 binding domain. Four conserved IWN repeats,

named for their central isoleucine, tryptophan, and asparagine residues, are dispersed throughout the protein, with two on either side of the central DNAJ-domain. These repeats are a defining feature of RME-8, found in all RME-8 homologs, but not other proteins.

The DNAJ domain is a 70 amino acid helical hairpin that recruits and activates the ATPase activity of Hsp70 enzymes. In Eukaryotes the Hsp70/DNAK protein family mediates local melting of three-dimensional protein structures. This activity promotes proper protein folding/refolding, solubilization of protein aggregates, assembly and disassembly of oligomeric structures, and translocation across membranes (reviewed in [25]).

The complexity and number of DNAJ domain proteins has increased tremendously over the course of evolution [21-23], with *C. elegans* having 34 members and Humans having over 50. The 260 kDa RME-8 protein is by far the largest DNAJ domain protein, most of which are small proteins of about 20 kDa. RME-8 is remarkably conserved throughout Eukarya with notable absences in Fungi and Gymnosperms.

While RME-8 represents an important endosomal regulator balancing recycling and degradative activities, how RME-8 itself is regulated has been unclear. We previously noted evidence for a physical interaction between the RME-8 DNAJ domain and sequences C-terminal to the RME-8 DNAJ domain. We posited that the RME-8 C-terminus could occlude the productive DNAJ domain interaction with Hsc70. Another clue to RME-8 regulation is our previous observation that RME-8 and SNX-1 physically interact, with neither appearing to depend upon the other for endosomal recruitment [9-11].

In this study we identify new regions of interest conserved across phyla. Using structure function

analysis, we show that the C-terminus of RME-8 both forms an inhibitory RME-8 C-terminus/ DNAJ domain interaction and controls microdomain segregation *in vivo*. Furthermore, we provide evidence that mutants in the IWN3 domain, but not IWN4, are hyperactive in uncoating ESCRT-0. Combining structural modeling with RME-8 mutagenesis and *in vivo* microdomain analysis we propose a model whereby SNX-1 disrupts an inhibited conformation of RME-8 mediated by its own IWN domains. We posit that this disruption is needed for productive exposure of the DNAJ domain for uncoating of both its own activator, SNX-1, and ESCRT-0 microdomains.

RESULTS

RME-8 has ancient origins, high conservation of key domains, and new regions of interest

To better understand RME-8 and its domains we comprehensively analyzed its evolutionary conservation in the 4000 predicted proteomes available at NCBI. We used *C. elegans* RME-8 as a query for a BLAST search, then filtered for >40% query coverage and <1E-3 e-value (see Methods). We found that RME-8 is scattered among Eukarya, as homologs are found in a diverse array of protists, such as the orphan protist lineage *Guillardia theta,* and in both free-living and parasitic protists such as *Entamoeba* and *Dictyostelium*, but absent in *Trichomonas, Giardia* and Alveolates (Figure 1A). Interestingly, RME-8 is completely absent from Fungi, but present in the closely related *Choanoflagellates* and Sponges. Additionally, RME-8 is mostly present in Plants except for Gymnosperms. This pattern suggests an ancient origin for RME-8, with selective loss in specific lineages.

Given the broad array of sequences compared, our analysis narrows and illuminates key domains in RME-8. Not surprisingly the DNAJ-domain is a highly conserved feature, as DNAJ

domains are ancient and widely conserved in all kingdoms of life (Figure 1B and 1C, and 1S). Despite being well conserved in animals, both the extreme N-terminal lipid binding domain, as defined by [29], and the IWN1 repeat, display low sequence conservation across Eukarya. The IWN2, IWN3 and IWN4 repeats, however, display strong conservation throughout Eukarya (Figure 1C). The regions from the RME-8 N-terminus to just before IWN2 are much less conserved than the remaining C-terminal sequences (Figure 1C). Moreover, the Parkinson's associated residue N855 is only conserved in animals (Figure 1C).

Our analysis also reveals new areas of interest outside of the defined functional domains. Specifically, residues just adjacent to IWN2 are highly conserved, as are sequences between the DNAJ-domain and IWN3. Additionally, the region between IWN3 and IWN4 displays strong conservation (See figure 1C and 1S). In the current study we set out to better understand the function of the IWN domains of RME-8 with respect to their role in controlling endosomal microdomains. Furthermore, we propose potential functions for the newly highlighted regions and IWN 2-4 domains.

The RME-8 IWN regions are important for membrane localization and microdomain positioning

120 The position of endosomes is stereotyped in the six specialized *C. elegans* scavenger cells
121 called coelomocytes. RAB-5 marked early endosomes are located toward the periphery of the
122 radially symmetrical disc shaped coelomocyte (Figure 2B, illustrated in 2A). RAB-7 marked late
123 endosomes and lysosomes localize more toward the interior (Figure 2C, illustrated in 2A)
124 [2][30]. The Golgi forms dispersed ministacks typical of invertebrate cells, and the nucleus is
125 positioned centrally (See Figure 2A). RME-8 localizes to recycling microdomains of the early
126 endosomes, most easily observed in coelomocytes because their endosomes are naturally quite
127 large (1-5 micron diameter) [9,10]. We find that the bulk of RME-8 microdomains on peripheral
128 endosomes are oriented toward the plasma membrane (Figure 2D).
129
130 To further study the role of the IWN-domains for RME-8 function *in vivo*, we created a series of
131 deletion transgenes that express tagged RME-8 missing certain IWNs and their surrounding
132 sequences (Illustrated in Figure 2G and S2). We measured how the RME-8 truncations
133 compared to wild-type in their ability to localize to discrete microdomains on endosomes of the
134 coelomocyte. RME-8 retaining the established lipid binding domain [29] but missing intervening
135 sequence before the J-domain, is less membrane localized than wild-type RME-8, with more
136 diffuse labeling in the cytoplasm (Figure 2E, quantified in 2H). This result suggests that N-
137 terminal sequences outside of the previously defined lipid binding domain contribute to
138 endosomal recruitment (see below). Interestingly, the remaining endosomal localization that did
139 occur in these deletion mutants still segregated into peripherally facing microdomains like wild-
140 type RME-8 (Figure 2D and C, quantified in 2I). Taken together these results suggest that the
141 N-terminal amino acids containing IWN1 and IWN2 repeats (aa100-1321) (See figure 1B) play a
142 role in membrane association, but do not control RME-8 microdomain localization.
143
144 In stark contrast, RME-8 lacking the C-terminal IWN3 and/or IWN4 regions displayed both more

intense endosome localization, and broader spread on the endosomal limiting membrane (Figure 2D, 2F, quantified in 2H, 2I, and S2). Moreover, the physically distinct recycling and degradative microdomains become mixed in the RME-8 IWN3 and/or IWN4 deletion strains (Figure 3E, 3G, illustrated in 3I, quantified in 3H). While the localization of RME-8 C-terminal truncation mutant protein spreads around the endosome, tagged SNX-1 remained in peripheral microdomains in these strains (Figure 3A, 3C, illustrated in 3I, quantified in 3D).

Taken together, these results indicate that the RME-8 sequences N-terminal to the DNAJ domain, and sequences C-terminal to the DNAJ domain, have distinct functions. N-terminal sequences well beyond the previously proposed lipid binding domain contribute to membrane association, but not microdomain segregation. The microdomain segregation function requires both the IWN3 and IWN4 regions, as loss of either leads to RME-8 spreading around the endosome and microdomain mixing. Moreover, given that deletion of IWN3 or IWN4 regions leads to increased membrane localization, as measured by membrane to cytoplasm ratio (Figure 2H), IWN3 and IWN4 regions may contribute to removal of RME-8 from the endosome as it cycles on and off the membrane.

The RME-8 IWN3 and IWN4 regions are required for RME-8 to uncoat ESCRT-0

A significant role for RME-8 in directing cargo sorting is to limit the growth of the degradative microdomain. Moreover RME-8 prevents the degradative machinery from entering the recycling microdomain, consequently limiting degradation of endocytosed cargo that should recycle [10]. In the absence of RME-8, ESCRT-0 component HRS/HGRS-1 over accumulates on the endosomes, and mixes with the recycling domain [10].

We found that RME-8 mutants lacking IWN3 and IWN4 regions fail to rescue the HRS/HGRS-1

overaccumulation phenotype of *rme-8(b1023ts)* mutants (Figure 3K-N, quantified 3P). This inability to uncoat HRS/HGRS-1 occurs despite a marked increase in RME-8(ΔIWN3+ΔIWN4) spatial overlap with HRS/HGRS-1 (Figure 3G, quantified in 3H, illustrated in 3J). RME-8 N-terminal truncation (ΔIWN1+2), did however retain a very weak ability to uncoat HRS (Figure 3L, Quantified in 3P). We note that none of the truncation mutants of RME-8 appear fully functional, as they all fail to rescue the smaller coelomocyte size phenotype that occurs upon loss of RME-8 (Figure 3O).

The RME-8 DNAJ domain inhibits the SNX-1/RME-8 interaction

Our previous work indicated that RME-8 sequences C-terminal to the DNAJ domain interact with both the RME-8 DNAJ domain and to the helical BAR domain of SNX-1 [9]. We postulated that SNX-1 binding to RME-8 C-terminal sequences may compete with the RME-8 C-terminal sequence binding to the RME-8 DNAJ domain, contributing to DNAJ domain regulation (See Figure 4I). Consistent with such a competition, we found that the presence of the DNAJ domain decreased the RME-8/SNX-1 interaction as assayed by yeast two-hybrid (Figure 4A, S4). This result held true using either a minimal region that only includes the IWN3 region, or the optimal region that includes both IWN3 and IWN4 domains (Figure 4A, S4). Taken together these results supports the hypothesis that the SNX-1 domain competes with the RME-8 C-term/DNAJ interaction and is consistent with an *in vivo* role for SNX-1 in activating RME-8 by increasing the availability of the DNAJ domain to interact with substrates.

Charge reversals in IWN4 and IWN3 alter the RME-8 C-terminus/SNX-1 and RME-8 C-terminus/DNAJ interactions

To further understand this potential competition, we sought to identify key residues in RME-8 that mediate the DNAJ versus SNX-1 interactions. To this end, we used error prone PCR to

create a library of random mutations in RME-8 C-terminal to the DNAJ domain and screened for those mutations that imparted improved interaction with SNX-1 in yeast 2-hybrid. The RME-8 C-terminal fragment containing the DNAJ-domain paired with SNX-1 grows on the less stringent assay media SC-HIS (Figure S3), indicating an interaction, but, importantly, does not grow on the more stringent assay media SC-URA (Figure 4B). This difference enabled selection for putative improved RME-8/SNX-1 binding mutants on SC-URA. Given that in PCR mutagenesis the most common errors are premature stop codons and frame shifts, selecting for an improved SNX-1 interaction enriches informative full-length RME-8 point mutants.

This screen yielded two mutants (E1962K and N1966K), both of which altered residues in the IWN4 domain of RME-8. Suggesting that charge may play a role, both mutations replaced an acidic residue (E1962) or a polar residue (N1966) with the basic residue lysine (Figure 4B and 4D). Likewise, further tests showed that replacing E1962 with arginine also led to growth of the RME-8 bait with SNX-1 BAR domain prey on the SC-URA stringent assay media (Figure 4B). This result suggests that the charge of the IWN4 region is important. Importantly, a separate pulldown assay showed that the IWN4 E1962K mutation significantly reduced binding between the DNAJ domain and the IWN3-IWN4 containing fragment of RME-8, an unselected effect. This result is consistent with our hypothesis that IWN4 mutations are improving SNX-1 binding by reducing a competing binding reaction with the RME-8 DNAJ domain (Figure 6E).

Given the IWN3 central positioning in the minimal SNX-1 binding domain, as well as its similarity to IWN4, we also tested similar charge reversals of acidic residues in IWN3. We found that introduction of a D1657K mutation in IWN3 also reduced interaction between the DNAJ domain and the IWN3-IWN4 containing domain (Figure 4C). However, unlike with IWN4, D1657K mutation in RME-8 IWN3 did not alter the RME-8/SNX-1 interaction (Figure 4B). Taken together

these data support the idea that the acidic residues of IWN4 and IWN3 are important for a DNAJ domain/RME-8 C-term self-interaction.

Charge reversals near the DNAJ domain active site also alter the RME-8/SNX-1 interaction

If the acidic residues of IWN4 and IWN3 mediate an electrostatic interaction with the DNAJ domain, we would expect to find complementary basic residues in the DNAJ-domain that would have a similar role in informing the SNX-1/RME-8 interaction. Indeed, several lysine and arginine residues on helix II of all DNAJ domains create a surface exposed basic patch (shown in blue) adjacent to the catalytic HPD residues that reside between helix II and III (figure 4E [21,31-33]). This basic patch has been implicated in Hsc70 binding to DNAJ domains, and thus any domain interactions with this patch could regulate Hsc70 activation [32,34].

With an analogous strategy to that which identified the IWN4 mutants, we targeted the lysines and arginines (figure 4F) of helix II and III in the predicted RME-8 DNAJ-domain basic patch (Figure 4E). We used doped oligo directed mutagenesis to screen for an improved RME-8/SNX-1 interaction (See methods). Transformants were selected on SC-URA and sequenced. The arginine residues of the DNAJ-domain were screened in a separate but similar fashion.

Our screen identified a K1347E/K1356E double mutant that produced robust growth on SC-URA (Figure 4F). Analogous residues in the *E. coli* DnaJ protein were found to both contribute to DNAK(Hsc70) binding and to be important for the DNAJ *in vivo* activity [32,34]. After a week of growth on SC-URA the R1342E/R1343E double mutant, that displayed some growth (Figure S4), suggesting that the basic nature of the DNAJ domain is important.

If the improved SNX-1 binding of these DNAJ-domain mutants is due to a disruption of the

246 RME-8 C-terminus/DNAJ-domain self-interaction, we would expect these mutants to display
247 decreased ability to bind to the RME-8 C-terminus. To this end we performed a pull-down assay
248 in which GST tagged wild-type or mutant DNAJ domain was used as bait with RME-8(1388-
249 2279) prey. We found that the charge reversals in the DNAJ domain weakened its interaction
250 with the RME-8 C-terminus (Figure 4G,H). These results suggest that K1347E and K1356E
251 depress the RME-8 self-interaction in favor of an RME-8/SNX-1 interaction (See 4I for
252 illustration).
253
254 **RME-8 D1657K (IWN3*) is hyperactive for uncoating HRS/HGRS-1**
255 A key function of RME-8 and SNX-1 is to limit the assembly of the ESCRT-0 microdomain [10].
256 Hence, we tested the functionality of our newly identified IWN3 and IWN4 altered alleles of
257 RME-8 *in vivo.* Importantly, we found a significant reduction of HRS/HGRS-1 on endosomes in
258 transgenic animals expressing the RME-8(IWN3*) D1657K mutant, but not in IWN4*(Figure 5A-
259 C'', quantified in 5E). Since this is the opposite effect of *rme-8* loss-of-function, these results
260 indicate that RME-8(IWN3*) is hyperactive.
261 This hyperactivity can likely be attributed to reduced inhibition of the DNAJ domain when IWN3
262 is mutated. Importantly, RME-8(IWN3*) also shows increased overlap with the normally
263 physically distinct ESCRT-0 microdomain, consistent with more HRS/HGRS-1 engagement and
264 disassembly (Figure 5A-C", quantified in 5D, illustrated in 5F). Conversely, *in vivo* we observe
265 SNX-1 colocalization with RME-8 is dramatically lower for RME-8(IWN3*) than with wild-type
266 RME-8 (Figure 6F-G", quantified in 6J, illustrated in 6K). Our results for IWN4 mutants, that
267 display an increase in SNX-1 binding, were different. Indeed, none of these altered HRS/HGRS-
268 1 accumulation (Figure 5C" and S4, quantified in 5E and S4). We tested CRISPR mediated
269 endogenous alterations E1962K, and a triple lysine substitution at E1959, E1962, or N1966
270 (Figure S5). We also tested the IWN4* transgene E1959, E1962, E1967 (Figure 5C"). Taken

271 together these results suggest that RME-8 may in part act independently of SNX-1 for
272 degradative domain uncoating activity.

273

274 **RME-8(+) can regulate RME-8(IWN3*)**

275 Interestingly, the hyperactivity of RME-8(IWN3*) in reducing HGRS-1/Hrs levels on endosomes
276 was blocked by endogenous wild-type RME-8, since we only observed this hyperactivity of
277 RME-8(IWN3*) when endogenous RME-8 was removed by temperature shift of *(b1023ts)*
278 mutants (Figure 5A" and B", quantified in 5E). As mentioned above, the microdomain positioning
279 of the hyperactive RME-8(IWN3*) shows more overlap with HGRS-1/Hrs (Figure 5A-C,
280 quantified in 5D, illustrated in5F), and is shifted internally, away from the plasma membrane
281 (Figure 6B and 6D, quantified in 6I, illustrated in 6J). This effect could be diminished by
282 overexpression on wild-type RME-8 (Figure 6E-F" quantified in 6I, illustrated in 6L). The ability
283 of wild-type RME-8 to inhibit the increased uncoating activity of RME-8(IWN3*), and to affect the
284 localization of RME-8(IWN3*), suggests that RME-8 may homo-oligomerize, with wild-type
285 RME-8 able to bind and inhibit RME-8(IWN3*).

286

287 **RME-8 endosomal positioning is also altered by expression level and SNX-1**

288 RME-8(+) displays a very peripheral and clumpy microdomain localization in *snx-1(0)* mutants,
289 the opposite microdomain localization of RME-8(IWN3*) (Figure 6C and 6D, quantified in 6I,
290 illustrated in 6J). These differences suggest that while at some point in its activation cycle RME-
291 8 may act independently of SNX-1, SNX-1 still strongly influences RME-8 localization and
292 activation. Indeed, the increased peripheral localization of RME-8(+) in *snx-1(0)* mutants is
293 similar to higher levels of RME-8(+) overexpression (Figure 6E-E"). This result supports the idea
294 of a competition between SNX-1 binding and RME-8 self-binding. These results also appear

more compatible with RME-8 self-interactions occurring via homodimers rather than self-interaction within one molecule.

RME-8 regulates SNX-1 dynamics

RME-8 and SNX-1 are binding partners, and both potentiate retrograde recycling and the separation of degradative and recycling microdomains on sorting endosomes [9,10]. The optimal SNX-1 binding domain of RME-8 encompasses IWN3 and IWN4 (Figure 4A). Indeed, without IWN3, IWN4, or both, RME-8 and SNX-1 display reduced overlap and appear disengaged (Figure 3C, quantified in 3D, illustrated in 3I) as RME-8 lacking these sequences does not segregate into a microdomain, but rather spreads throughout the endosome (Figure 3C, quantified in 3F, illustrated in 3G). In mammalian cells when RME-8 is depleted by siRNA, mammalian Snx1 accumulates on endosome associated membrane tubules [35]. Similarly, we observe SNX-1 overaccumulation on endosomes in *rme-8(b1023ts)* mutants at restrictive temperature (Figure 7A, quantified in 7F). Unlike IWN3* and WT, none of the RME-8 domain deletion mutants can rescue SNX-1 overaccumulation in *rme-8ts* mutant animals (Figure 7C and D, quantified in 7F). Moreover, the size of SNX-1 microdomains are diminished rather than enlarged in the RME-8(IWN3*) expressing animals (Figure 7E, quantified in 7G). Not only does SNX-1 over accumulate in the absence of RME-8, but recovery after photobleaching of GFP-SNX-1 on endosomes is much slower than wild-type, never recovering to the levels found in animals expressing wild-type RME-8 within the time-frame monitored (Figure 7H-I’’’, quantified in 7J). These results suggest that SNX-1 may be a substrate for RME-8/Hsc70 assembly/disassembly activities, in addition to acting as an activator of RME-8 uncoating activity toward the degradative microdomain.

DISCUSSION

Endosomes are organelles that play an essential role in protein and lipid sorting in all eukaryotic cells. Over the past 20 years evidence has emerged that microdomains of endosomal limiting membranes are key features of endosomes, with specific coat complexes representing competitive activities of the endosome that define these microdomains. Physical self-associations and/or oligomerization as is seen with HRS/HGRS-1 can partially explain the segregation of microdomains (For review see [11]). Additional cross-regulatory interactions between degradative and recycling microdomains also occur [9,10,36], but little is known of the molecular mechanisms that separate these coat complexes to maintain efficient endosome function. In our previous work we identified RME-8 as a key protein in this process, acting to keep recycling and degradation in balance**.**

Recycling microdomain components and binding partners RME-8 and SNX-1 are required to limit the assembly of the opposing degradative microdomain. The pair likely act by disassembling ESCRT-0 complexes that encroach into the recycling domain where they could interfere with recycling. Here we sought to better understand how the large and complex RME-8 protein functions using structure-function analysis. In this study we define a role for sequences N-terminal to the DNAJ domain in endosomal recruitment. We also extend our previous model suggesting that an interaction between the DNAJ domain and sequences C-terminal to it regulate RME-8 activity.

Predicted structure of RME-8 via AlphaFold

During the late phases of completing this manuscript, a new highly lauded AI-based system for

345 protein structure prediction, called AlphaFold, was released. Thus, we sought to analyze the
346 AlphaFold predicted structure for *C. elegans* RME-8 (see
347 https://AlphaFold.ebi.ac.uk/entry/G5ED36) with respect to our structure-function results [37].
348 The predicted structure shows an N-terminal domain that is enriched in beta-sheets (Figure 8H
349 and see below). Outside of the N-terminal first 400 amino acids, much of the predicted RME-8
350 structure consists of a series of 5 alpha-solenoids containing HEAT repeats, with short linkers
351 between them (Figure 8A-D). Remarkably, these linkers correspond to the RME-8 IWN domains
352 (IWN domains denoted in blue 8A,B and 8E-G). AlphaFold also predicts that the small DNAJ
353 domain protrudes from RME-8, extending from the 3rd alpha-solenoid back toward the 2nd
354 alpha-solenoid, positioned adjacent to IWN2 (Figure 8A and B). We colored the predicted 3-
355 dimensional structure according to our pan-Eukarya conservation analysis from Figure 1 and S1
356 (Figure 8C and 8D). This conservation analysis indicates that in addition to IWN2, the regions
357 outside of, but adjacent to, IWN2 and DNAJ might contribute to this DNAJ domain orientation
358 (see yellow arrows Figure 1 and 1S). Moreover, a region encompassing solenoid S3, S4, and
359 part of S5 is highly conserved.
360

361 **RME-8 N-terminus has three PH-like domains rather than one**

362 Previous work indicated that human RME-8 contains an N-terminal PH-like domain, similar to
363 the PH-domain of FERM1 [29] (Figure 8I). This domain was shown to preferentially bind
364 membranes enriched in PI(3)P and PI(3,5)P2, phosphoinositides well known for recruiting
365 peripheral membrane proteins to early and late endosomes [29]. Our new *in vivo* structure-
366 function analysis indicated additional adjacent sequences in RME-8 beyond this region that
367 contribute to endosome recruitment (Figure 2E).
368

369 While not apparent in the primary sequence, using the Pymol™ align feature to our analyze of

the AlphaFold predicted structure, we identified two additional PH-like domains within the first 400 amino acids of RME-8 (Figure 8H-I). All three predicted PH-like domains, including the previously described domain at the extreme N-terminus, are structurally similar to the FERM1 PH domain (Figure 8H-I). A requirement for the two additional predicted PH-like domains provides a simple explanation for our results showing a requirement for additional sequences in this region of RME-8 for efficient membrane recruitment (Figure 2E quantified in 2H). Taken together these results suggest three PH-like domains may work in concert to direct RME-8 to the endosomal membrane via phosphoinositide lipid binding.

IWN motifs as conformational control points in autoinhibition

As described above, the AlphaFold prediction suggests that the bulk of RME-8 consists of a series of 5 alpha-solenoids with short linkers between them (Figure 8A). These linkers between solenoids are predicted to lie within the IWN motifs, where they are predicted to occur as short beta-strands that terminate an alpha-helix (Figure 8A and 8D, 8E). The IWN tryptophan residue is predicted to be buried and surrounded by hydrophobic residues (Figure 8F). The isoleucine and asparagine, however, are predicted to be on the opposite side of the beta strand, both interacting with nearby peptide backbone features. We find that all four IWNs display similar predicted secondary and tertiary structure (Figure 8D). In the Case of IWN3, the aspartic acid 1657 that is mutated to lysine in IWN3*, is predicted to interact with the adjacent alpha-helix (Figure 8G). A substitution of lysine at this position would likely be quite disruptive to the orientation of the third and fourth solenoids.

The prediction that the conserved IWN repeats represent linkers between domains supports the idea that the IWN motifs control large scale conformational changes in RME-8. This is consistent with our new data that sequences in RME-8 C-terminal to the DNAJ domain contain

395 autoinhibitory activity, especially our finding that a single point mutation in IWN3 is sufficient to
396 produce a hyperactive protein, and that IWN3 and IWN4 regions of the protein physically
397 interact with the DNAJ domain. We currently favor a model in which the relevant autoinhibitory
398 interactions between IWN3-IWN4 and the DNAJ domain occurs between RME-8 molecules in
399 an oligomer, rather than within a single RME-8 molecule. In particular, our finding that wild-type
400 RME-8 can inhibit the hyperactivity and alter the microdomain positioning of the IWN3* mutant
401 version of RME-8 could be explained if oligomerized RME-8 molecules are autoinhibited.
402
403 **The role of SNX-1**
404 We have previously proposed that SNX-1 is a positive regulator of RME-8 as loss of either SNX-
405 1 or RME-8 has similar effects on cargo recycling and expansion of the degradative
406 microdomain [10]. Our model predicts that SNX-1 binding derepresses RME-8, allowing RME-8
407 to uncoat both ESCRT-0 and, intriguingly, SNX-1 itself. If oligomerization of RME-8 inhibits
408 activity, then SNX-1 binding could act to release active RME-8 monomers that can work with
409 Hsc70 to disassemble both SNX-1 and ESCRT-0 complexes (Figure 9B).
410
411 According to this model, when the RME-8/DNAJ interaction is reduced, as in the case of IWN3*,
412 more RME-8 can de-oligomerize and shift its positioning to invade the degradative
413 microdomain, leading to the hyperactive uncoating of HRS/HGRS-1 that we observe with
414 IWN3*(Figure 9B and 9E). As with IWN3*, IWN4* also reduces RME-8/DNAJ interaction, but the
415 interaction with SNX-1 is different. IWN4* improves the interaction with SNX-1 and is *not*
416 hyperactive hinting that release of SNX-1 maybe an important part of the activation cycle of
417 RME-8.
418
419 Results are also different when large portions of the C-terminal regions encompassing IWN3 are

fully deleted, a situation where we expect that RME-8 also cannot bind to SNX-1 or self-oligomerize. In this case we do observe spreading of nonfunctional RME-8 around the endosome (Figure 9C). This difference between the IWN3* point mutation and full domain deletion indicates another essential function of RME-8 sequences after the DNAJ domain beyond autoinhibition.

In addition to stimulating Hsc70 ATPase activity, substrate binding is a typical function of DNAJ domain proteins. Because DNAJ-domain cochaperones typically act as cargo adapters for Hsc70, the RME-8 C-terminus is likely binding Hsc70 substrate(s). It is still unclear what the direct substrate of RME-8/Hsc70 is that controls the degradative microdomain. Candidate substrates include ESCRT-0 components HGRS-1/Hrs or STAM, Clathrin that associates with ESCRT-0, or other associated molecules, but clear identification of the key substrate awaits further studies.

New data presented in this work, along with published observations on RME-8 siRNA phenotypes in mammalian cells, also suggests that SNX-1 itself is a good candidate to be a substrate for RME-8/Hsc70 chaperone activity. Observations as to the importance of RME-8 for control of endosomal SNX-1 has been previously reported by Freeman et al. [34]. This work showed that relatively static Snx1 coated endosomal tubules accumulated after treatment of Hela cells with RME-8 siRNA. Consistent with these findings, we show that SNX-1 accumulates on endosomes in an *rme-8ts* mutant, a phenotype that is rescued by IWN3* but not by defective RME-8 truncation transgenes (Figure 7). Additionally, FRAP analysis of SNX-1 positive endosomes shows that recovery of GFP::SNX-1 is dramatically slowed in the absence of RME-8 (figure 7). RME-8 activation by SNX-1 could be transient if the activation of the RME-8 DNAJ-domain ultimately terminates interaction of SNX-1 with RME-8, causing reversion of RME-8 to

445 the autoinhibited state (Figure 9). This strategy of activation of a powerful regulator tied to
446 inactivation is a common theme in membrane trafficking. Indeed SNX-1 being required for RME-
447 8 activation as well as a target of RME-8 disassembly activity could effectively localize the
448 powerful Hsc70 activity to the proper place and time.

449

450 We envision the SNX-1/RME-8 network in the recycling microdomain as part of a larger system
451 that acts to create and separate functional microdomains on endosomes, with likely feedback
452 regulation going in both directions. More work will be required to understand how the protein
453 complexes within microdomains act to balance the activities of the endosome to allow correct
454 sorting of incoming molecules and rebalance such activities as loads and cargo types change
455 over time. The *C. elegans* coelomocyte provides an excellent system to answer such questions.

456

457 **MATERIALS AND METHODS**

458

459 All *C. elegans* strains were derived originally from the wild-type Bristol strain N2. Worm cultures,
460 genetic crosses, and other *C. elegans* husbandry were performed according to standard
461 methods [38]. A complete list of strains used in this study can be found in Supplementary Table
462 1.

463

464 **Yeast Two-Hybrid Mutagenesis Screen**

465 We used error prone PCR [38,39] of RME-8 cDNA encoding amino acids 1322-2279 (J-domain
466 to C-terminus) in PDEST32™, followed by gap repair transformation. Mutagenized RME-8
467 fragments were co-transformed with a gapped vector, that included 100 bp homology arms, into
468 JDY27 yeast expressing SNX-1 amino acids 221-472 (BAR domain) in PDEST22™. JDY27 is a
469 yeast strains that includes several genomic reporter genes dependent on the Y2H interaction,

including ADE-2 and LacZ color assays, as well as HIS-3 and URA-3 growth assays (ade2-101 trp1-901 leu2-3.112 his3Δ200 ura3-52 gal4Δ gal80Δ SPAL::URA3 LYS2::GAL1-HIS GAL2-ADE2 met2:GAL7-LacZ (or GAL1-LacZ) can1R alpha). Approximately 10,000 transformed yeast were then plated on SC-HIS-LEU-TRP media and allowed to grow for 3 days at 30°C. These colonies were then replica plated to selective media SC-HIS-LEU-TRP-URA and allowed to grow for 10 days at 30°C. The 104 colonies that displayed an initial URA+ phenotype were patched onto SC-HIS-LEU-TRP-URA and selected for robust growth after 3 days at 30°C. We then retransformed the plasmids recovered from these colonies into the JDY27 SNX-1 strain to ensure the URA+ phenotype was dependent on the RME-8 plasmid. 30 colonies were then sequenced for mutations in the 1322-2279 region. Most colonies had multiple mutations, therefore we chose the strongest URA+ colonies to pursue, introducing mutations singly into PDEST32 RME-8 plasmids by site directed mutagenesis. We identified mutations E1962K and N1966K from two different colonies and chose to pursue their function further.

Yeast transformation and plasmid recovery

Yeast transformations were performed using cells grown in liquid 1x YPD overnight at 30°C. The pellet was then washed 1x with distilled water and resuspended in a solution of 0.1M LiOAc + 1x TE, at a 1:2 pellet size to buffer volume. 100ul of yeast slurry was then combined with 1µg of DNA and 10ul of denatured 10mg/ml salmon sperm DNA. Yeast were then incubated at 30°C for 30 minutes before adding 1ml 44% PEG + 0.1M LiOac and 1x TE, after which it was allowed to incubate for another 30 minutes at 30°C. Following this, DMSO was added at a 1:10 ratio to the PEG, and yeast were heat shocked in a 42°C water bath for 13 minutes. After the heat shock, yeast were spun down in a microcentrifuge and resuspended in 50µL 5mM $CaCl_2$ before being plated onto selective media.

Yeast plasmid recovery performed using QIAprep Spin Miniprep Kit and a user adapted

Protocol by Michael Jones, Chugai Institute for Molecular Medicine, Ibaraki, Japan. Essentially a colony of yeast is resuspended in 250ul of P1 buffer combined with 100 µl of acid-washed glass beads (Sigma G-8772) and vortexed for 5 min. The slurry is then used in the typical miniprep protocol, with the final eluate of the column used to transform bacteria for amplification of the plasmid DNA.

Homology searches

We used the NCBI BLAST to probe the over 4000 proteomes in the NCBI database for the existence of DNA J proteins that also contained IWN repeats. We used the *C. elegans* RME-8 amino acid sequence and the default BLAST algorithm to probe each taxonomic group for an RME-8 homolog. We filtered the results with a coverage threshold of >40% and e value < .001. We then hand curated each positive to ensure that it contained IWN repeats defined by I/L/V W ζ ζ, all of the hits with at least 40% coverage contained at least three of the IWN repeats.

Display of tree of life

To display the phylogenetic conservation of RME-8 we used iTOL version 5.7 [40] which is based on Tree of Life v1.0 [41].

Single Copy MiniMos transgenes

Plasmids for *C. elegans* coleomocyte expression were produced by standard methods including *in vitro* recombination via the Gateway system (ThermoFisher) and/or Gibson Assembly using the Nebuilder system (NEB). Plasmid backbones were pCFJ1662 and pCFJ910 (Addgene) and used promoters from the *snx-1* or *cup-4* genes. Our minimos protocol for single copy transgene integration is based on a protocol found on wormbuilder.org as described in [42]. The gonad arms of first day gravid adults were microinjected with plasmid mixtures including 10ng/ul drug resistant expression plasmid (G418 or Hygromycin) [43,44] 10ng/µl pGH8, 2.5ng/µl pCFJ90,

65ng/µl, and 10ng/ul pCFJ601. 2-3 injected animals per plate were incubated at 25°C, with selection drug added between 24-72 hrs post injection. Plates were screened for single copy integrated transformants after a minimum of 10 days of growth, focused on populations that survive drug selection and lack extrachromosomal arrays visualized with the mCherry co-injection markers. Candidate single-copy integrants were passaged on drug containing plates and analyzed for expression. Lines displaying 100% transmission of the expressed transgene without drug selection were frozen and used for experiments.

Microscopy and image analysis

Live animals were mounted on 10% agarose pads and immobilized using 0.1um polystyrene microspheres (Polysciences 00876-15) [45]. Multiwavelength fluorescence Z-series with 0.2 micron step size were obtained using a SOLA SE 365 Solid state light engine, Axiovert 200M (Carl Zeiss MicroImaging) microscope equipped with a digital CCD camera (QImaging; Rolera EM-C2), or Axio Observer (Carl Zeiss MicroImaging) microscope equipped with a scientific sCMOS camera (Photometrics Prime 95B), captured using MetaMorph 7.7 software (Universal Imaging) and then deconvolved using AutoDeblur X3 software (AutoQuant Imaging). Colocalization analysis was done using MetaMorph 7.7 colocalization plugin, whereby intensities in each channel were thresholded and Pearson's correlation was analyzed. Intensity measurements were also analyzed by MetaMorph 7.7, using thresholded images captured under identical acquisition parameters. FRAP was done as described in [9]

Graphing and statistics

Results were all graphed using GraphPad Prism 8.4.3 software and significance was measured by one-way ANOVA or students t-test.

[1] Grant B, Hirsh D: **Receptor-mediated Endocytosis in the Caenorhabditis elegans Oocyte**. MBoC 1999, 10: 4311-4326.

[2] Zhang Y, Grant B, Hirsh D: **RME-8, a conserved J-domain protein, is required for endocytosis in Caenorhabditis elegans**. Mol.Biol.Cell 2001, 12: 2011-2021.

[3] Silady RA, Ehrhardt DW, Jackson K, Faulkner C, Oparka K, Somerville CR: **The GRV2/RME-8 protein of Arabidopsis functions in the late endocytic pathway and is required for vacuolar membrane flow**. The Plant Journal 2008, 53: 29-41.

[4] Chang HC, Hull M, Mellman I: **The J-domain protein Rme-8 interacts with Hsc70 to control clathrin-dependent endocytosis in Drosophila**. Journal of Cell Biology 2004, 164: 1055-1064.

[5] Girard M, McPherson PS: **RME-8 regulates trafficking of the epidermal growth factor receptor**. FEBS Letters 2008, 582: 961-966.

[6] Xhabija B, Taylor GS, Fujibayashi A, Sekiguchi K, Vacratsis PO: **Receptor mediated endocytosis 8 is a novel PI(3)P binding protein regulated by myotubularin-related 2**. FEBS Lett. 2011, 585: 1722-1728.

[7] Girard M, Poupon V, Blondeau F, McPherson PS: **The DnaJ-domain protein RME-8 functions in endosomal trafficking**. J.Biol.Chem. 2005, 280: 40135-40143.

[8] Fujibayashi A, Taguchi T, Misaki R, Ohtani M, Dohmae N, Takio K, Yamada M, Gu J, Yamakami M, Fukuda M, et al.: **Human RME-8 is involved in membrane trafficking through early endosomes**. Cell Struct.Funct. 2008, 33: 35-50.

570 [9] Shi A, Sun L, Banerjee R, Tobin M, Zhang Y, Grant BD: **Regulation of endosomal clathrin**
571 **and retromer-mediated endosome to Golgi retrograde transport by the J-domain protein**
572 **RME-8**. EMBO J. 2009, 28: 3290-3302.

573 [10] Norris A, Tammineni P, Wang S, Gerdes J, Murr A, Kwan KY, Cai Q, Grant BD: **SNX-1 and**
574 **RME-8 oppose the assembly of HGRS-1/ESCRT-0 degradative microdomains on**
575 **endosomes**. Proc.Natl.Acad.Sci.U.S.A. 2017, 114: E307-E316.

576 [11] Norris A, Grant BD: **Endosomal microdomains: Formation and function**. Current opinion
577 in cell biology 2020, 65: 86-95.

578 [12] Seaman MN, Harbour ME, Tattersall D, Read E, Bright N: **Membrane recruitment of the**
579 **cargo-selective retromer subcomplex is catalysed by the small GTPase Rab7 and**
580 **inhibited by the Rab-GAP TBC1D5**. J.Cell.Sci. 2009, 122: 2371-2382.

581 [13] Liu T, Gomez TS, Sackey BK, Billadeau DD, Burd CG: **Rab GTPase regulation of**
582 **retromer-mediated cargo export during endosome maturation**. Molecular biology of the cell
583 2012, 23: 2505-2515.

584 [14] Rojas R, van Vlijmen T, Mardones GA, Prabhu Y, Rojas AL, Mohammed S, Heck AJR,
585 Raposo G, van der Sluijs P, Bonifacino JS: **Regulation of retromer recruitment to**
586 **endosomes by sequential action of Rab5 and Rab7**. Journal of Cell Biology 2008, 183: 513-
587 526.

588 [15] Seaman MNJ: **The retromer complex - endosomal protein recycling and beyond**.
589 Journal of cell science 2012, 125: 4693-4702.

590 [16] Vilariño-Güell C, Rajput A, Milnerwood AJ, Shah B, Szu-Tu C, Trinh J, Yu I, Encarnacion M,
591 Munsie LN, Tapia L, et al.: **DNAJC13 mutations in Parkinson disease**. Human molecular
592 genetics 2014, 23: 1794-1801.

593 [17] Rajput A, Ross,JP, Bernales,CQ, Rayaprolu,S, Soto-Ortolaza,AI, Ross,OA, Gerpen,Jv,
594 Uitti,RJ, Wszolek,ZK, Rajput,AH, Vilariño-Güell,C: Short report. Social Wellbeing Agency, Toi
595 Hau Tāngata; 2020.

596 [18] Cullen PJ, Steinberg F: **To degrade or not to degrade: mechanisms and significance of**
597 **endocytic recycling**. Nat.Rev.Mol.Cell Biol. 2018, 19: 679-696.

598 [19] Zarouchlioti C, Parfitt DA, Li W, Gittings LM, Cheetham ME: **DNAJ Proteins in**
599 **neurodegeneration: essential and protective factors**. Philosophical Transactions of the
600 Royal Society B: Biological Sciences 2018, 373: 20160534.

601 [20] Hasegawa T, Yoshida S, Sugeno N, Kobayashi J, Aoki M: **DnaJ/Hsp40 Family and**
602 **Parkinson's Disease**. Front. Neurosci. 2018, 11.

603 [21] Kampinga HH, Craig EA: **The Hsp70 chaperone machinery: J-proteins as drivers of**
604 **functional specificity**. Nat Rev Mol Cell Biol 2010, 11: 579-592.

605 [22] Silver PA, Way JC: **Eukaryotic DnaJ homologs and the specificity of Hsp70 activity**.
606 Cell 1993, 74: 5-6.

607 [23] Qiu X-, Shao Y-, Miao S, Wang L: **The diversity of the DnaJ/Hsp40 family, the crucial**
608 **partners for Hsp70 chaperones**. Cell Mol Life Sci 2006, 63: 2560-2570.

609 [24] Kityk R, Kopp J, Mayer MP: **Molecular Mechanism of J-Domain-Triggered ATP**
610 **Hydrolysis by Hsp70 Chaperones**. Molecular Cell 2018, 69: 227-237.e4.

611 [25] Mayer M, Bukau B: **Hsp70 chaperones: Cellular functions and molecular mechanism**.
612 CMLS, Cell. Mol. Life Sci 2005, 62: 670-684.

613 [26] Genevaux P, Georgopoulos C, Kelley WL: **The Hsp70 chaperone machines of**
614 **Escherichia coli: a paradigm for the repartition of chaperone functions**. Molecular
615 Microbiology 2007, 66: 840-857.

[27] Lindquist S, Craig EA: **The Heat-Shock Proteins**. Annual Review of Genetics 1988, 22: 631-677.

[28] Gupta RS, Singh B: **Cloning of the HSP70 gene from Halobacterium marismortui: relatedness of archaebacterial HSP70 to its eubacterial homologs and a model for the evolution of the HSP70 gene**. J Bacteriol 1992, 174: 4594-4605.

[29] Xhabija B, Vacratsis PO: **Receptor-mediated Endocytosis 8 Utilizes an N-terminal Phosphoinositide-binding Motif to Regulate Endosomal Clathrin Dynamics**. J Biol Chem 2015, 290: 21676-21689.

[30] Poteryaev D, Fares H, Bowerman B, Spang A: **Caenorhabditis elegans SAND-1 is essential for RAB-7 function in endosomal traffic**. The EMBO Journal 2007, 26: 301-312.

[31] Kityk R, Kopp J, Mayer MP: **Molecular Mechanism of J-Domain-Triggered ATP Hydrolysis by Hsp70 Chaperones**. Molecular cell 2018, 69: 227-237.e4.

[32] Genevaux P, Schwager F, Georgopoulos C, Kelley WL: **Scanning Mutagenesis Identifies Amino Acid Residues Essential for the in Vivo Activity of the Escherichia coli DnaJ (Hsp40) J-Domain**. Genetics 2002, 162: 1045-1053.

[33] Szyperski T, Pellecchia M, Wall D, Georgopoulos C, Wüthrich K: **NMR structure determination of the Escherichia coli DnaJ molecular chaperone: secondary structure and backbone fold of the N-terminal region (residues 2-108) containing the highly conserved J domain**. PNAS 1994, 91: 11343-11347.

[34] Ahmad A, Bhattacharya A, McDonald RA, Cordes M, Ellington B, Bertelsen EB, Zuiderweg ERP: **Heat shock protein 70 kDa chaperone/DnaJ cochaperone complex employs an unusual dynamic interface**. PNAS 2011, 108: 18966-18971.

638 [35] Freeman CL, Hesketh G, Seaman MNJ: **RME-8 coordinates the activity of the WASH**
639 **complex with the function of the retromer SNX dimer to control endosomal tubulation**.
640 Journal of cell science 2014, 127: 2053-2070.

641 [36] Zhang J, Liu J, Norris A, Grant BD, Wang X: **A novel requirement for ubiquitin-**
642 **conjugating enzyme UBC-13 in retrograde recycling of MIG-14/Wntless and Wnt**
643 **signaling**. Molecular biology of the cell 2018, 29: 2098-2112.

644 [37] Jumper J, Evans R, Pritzel A, Green T, Figurnov M, Ronneberger O, Tunyasuvunakool K,
645 Bates R, Žídek A, Potapenko A, et al.: **Highly accurate protein structure prediction with**
646 **AlphaFold**. Nature (London) 2021, 596: 583-589.

647 [38] Brenner S: **The Genetics of CAENORHABDITIS ELEGANS**. Genetics 1974, 77: 71-94.

648 [39] Wilson DS, Keefe AD: **Random Mutagenesis by PCR**. Current Protocols in Molecular
649 Biology 2000, 51: 8.3.1-8.3.9.

650 [40] Letunic I, Bork P: **Interactive Tree Of Life (iTOL) v4: recent updates and new**
651 **developments**. Nucleic Acids Research 2019, 47: W256-W259.

652 [41] Ciccarelli FD, Doerks T, von Mering C, Creevey CJ, Snel B, Bork P: **Toward automatic**
653 **reconstruction of a highly resolved tree of life**. Science 2006, 311: 1283-1287.

654 [42] Frøkjær-Jensen C, Davis MW, Sarov M, Taylor J, Flibotte S, LaBella M, Pozniakovsky A,
655 Moerman DG, Jorgensen EM: **Random and targeted transgene insertion in Caenorhabditis**
656 **elegans using a modified Mos1 transposon**. Nat Methods 2014, 11: 529-534.

657 [43] Giordano-Santini R, Milstein S, Svrzikapa N, Tu D, Johnsen R, Baillie D, Vidal M, Dupuy D:
658 **An antibiotic selection marker for nematode transgenesis**. Nat Methods 2010, 7: 721-723.

659 [44] Lehner B, Garcia-Verdugo R, Semple JI: **Rapid selection of transgenic C. elegans using**
660 **antibiotic resistance**. Nature methods 2010, 7: 725-727.

661 [45] Kim E, Sun L, Gabel CV, Fang-Yen C: **Long-Term Imaging of Caenorhabditis elegans**

662 **Using Nanoparticle-Mediated Immobilization**. PLoS ONE 2013, 8: 53419.

663

664

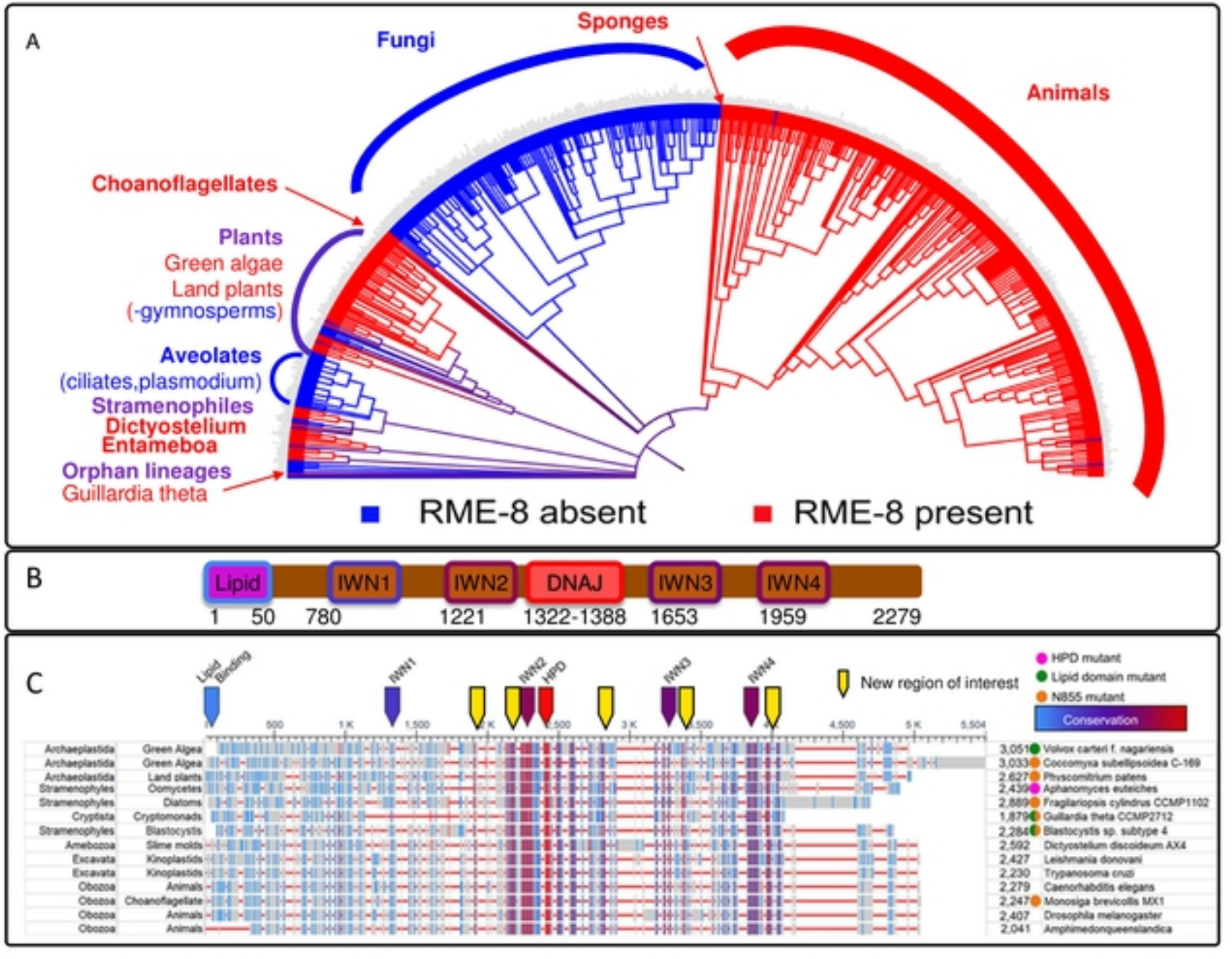

Figure 1. RME-8 homologs are found dispersed throughout Eukarya. (A) A phylogram of Eukarya generated in iTOL, (see methods). Branches containing an RME-8 homolog are indicated in red, nodes containing branches with RME-8 homologs present and absent are colored in purple, and branches or nodes containing no RME-8 homologs are colored in blue. (B) A schematic of RME-8 with key domains indicated. (C) An alignment of a sampling of RME-8 homologs from dispersed branches in Eukarya generated by the NCBI Multiple Sequence Alignment (MSA) viewer. The names of the phylogenetic categories are indicated to the left, and species names are indicated to the right of the MSA. Colored dots indicating mutations in key domains are indicated to the left of the species name. A pink dot indicates that key residues in the DNAJ domain are mutated. A green dot indicates the key W20 (human) residue in the originally proposed lipid binding domain is absent, and an orange dot indicates the Parkinson's associated residue N855 (human) is not conserved. In the MSA, red horizontal lines represent gaps, grey bars represent minimal homology, blue bars represent low homology and red indicates high homology. Arrows above the alignment indicate key areas of interest, known regions of interest are colored based on their homology, new regions of interest are indicated by yellow arrows.

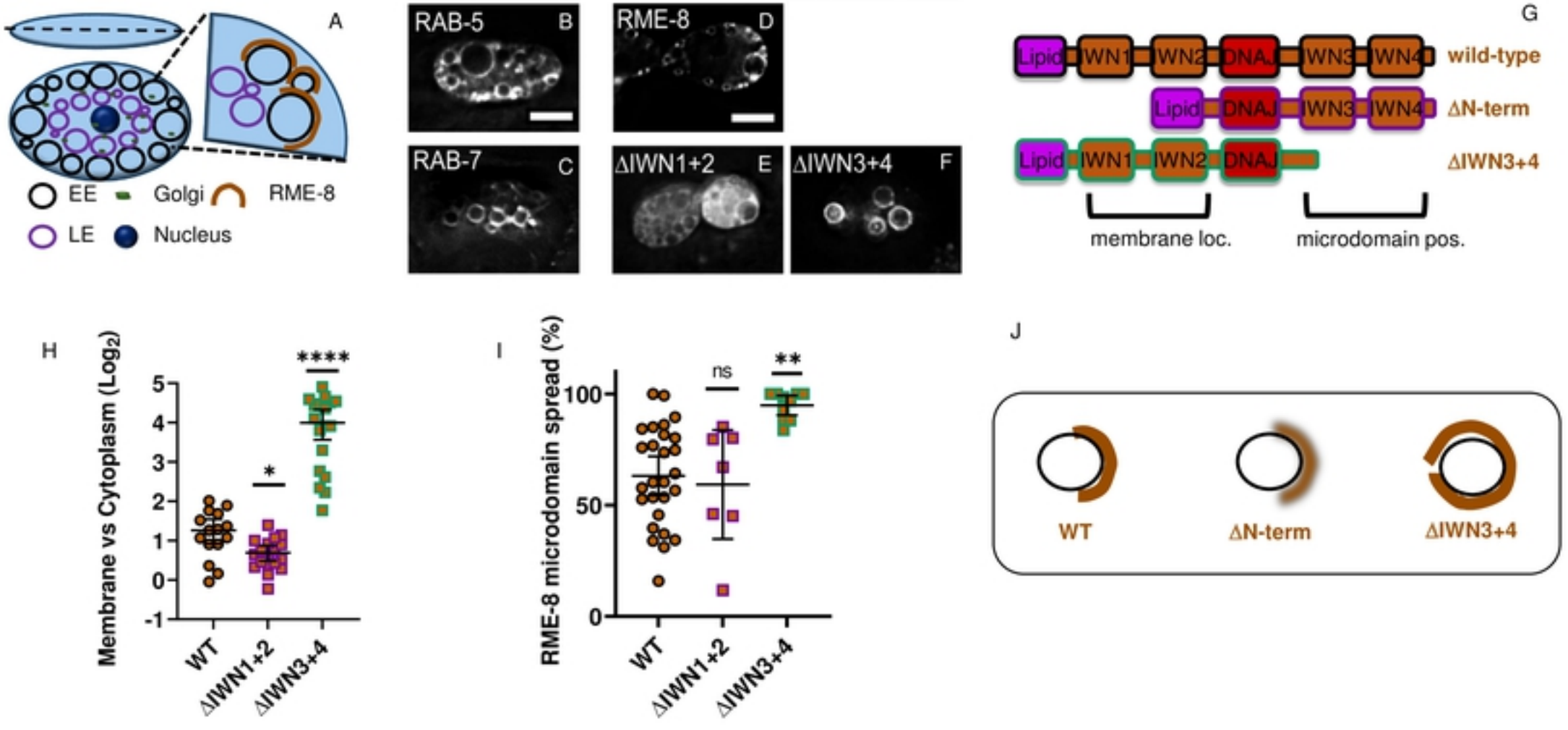
A
EE
Golgi
RME-8
LE
Nucleus
RAB-5
B
RME-8
D
RAB-7
C
ΔIWN1+2
E
ΔIWN3+4
F
G
Lipid
WN1
WN2
DNAJ
WN3
WN4
wild-type
ΔN-term
ΔIWN3+4
membrane loc.
microdomain pos.
H
Membrane vs Cytoplasm (Log2)
5
4
3
2
1
0
-1
*
****
WT
ΔIWN1+2
ΔIWN3+4
I
RME-8 microdomain spread (%)
100
50
0
ns
**
WT
ΔIWN1+2
ΔIWN3+4
J
WT
ΔN-term
ΔIWN3+4

Figure 2. The RME-8 N-terminus controls membrane association, while the C-terminus controls microdomain positioning, and microdomain spread. (A) Early endosomes (EE), Late endosomes (LE), Golgi, and the Nucleus occupy stereotypical positions in the coelomocyte cell. (B-C) Micrograph of tagRFP::RAB-5 (B) and tagRFP::RAB-7 (C) expressed in coelomocytes. (D-F) Micrograph of pSNX-1::GFP::RME-8 expressed in wild-type animals. Micrograph of pSNX-1::GFP::RME-8 N-terminal (E) and C-terminal truncations (F). (G) Illustration of wild-type, N-terminal and C-terminal truncations of RME-8. (H) Diagram of the coelomocyte segmented into peripheral and internal portions, and the calculation of the ratio of interior intensity to peripheral intensity. (J) Ratio of the GFP::RME-8 intensity in the cytoplasm versus on the membrane in the indicated GFP::RME-8 wild-type and truncations. The values are also plotted on a Log2 scale. (K) Quantification of the percentage of an endosome covered by the indicated GFP-RME-8 wild-type and truncation mutants. All micrographs are deconvolved widefield images (see methods). In I-K each data point is an individual worm, error bars indicate Mean with 95% CI, ANOVA statistical analysis done in Graphpad Prism with $p<0.5$=*, $p<0.01$=**, $p<0.001$=***, $p<0.0001$=****. Scale bars are 5 microns in whole coelomocyte images.

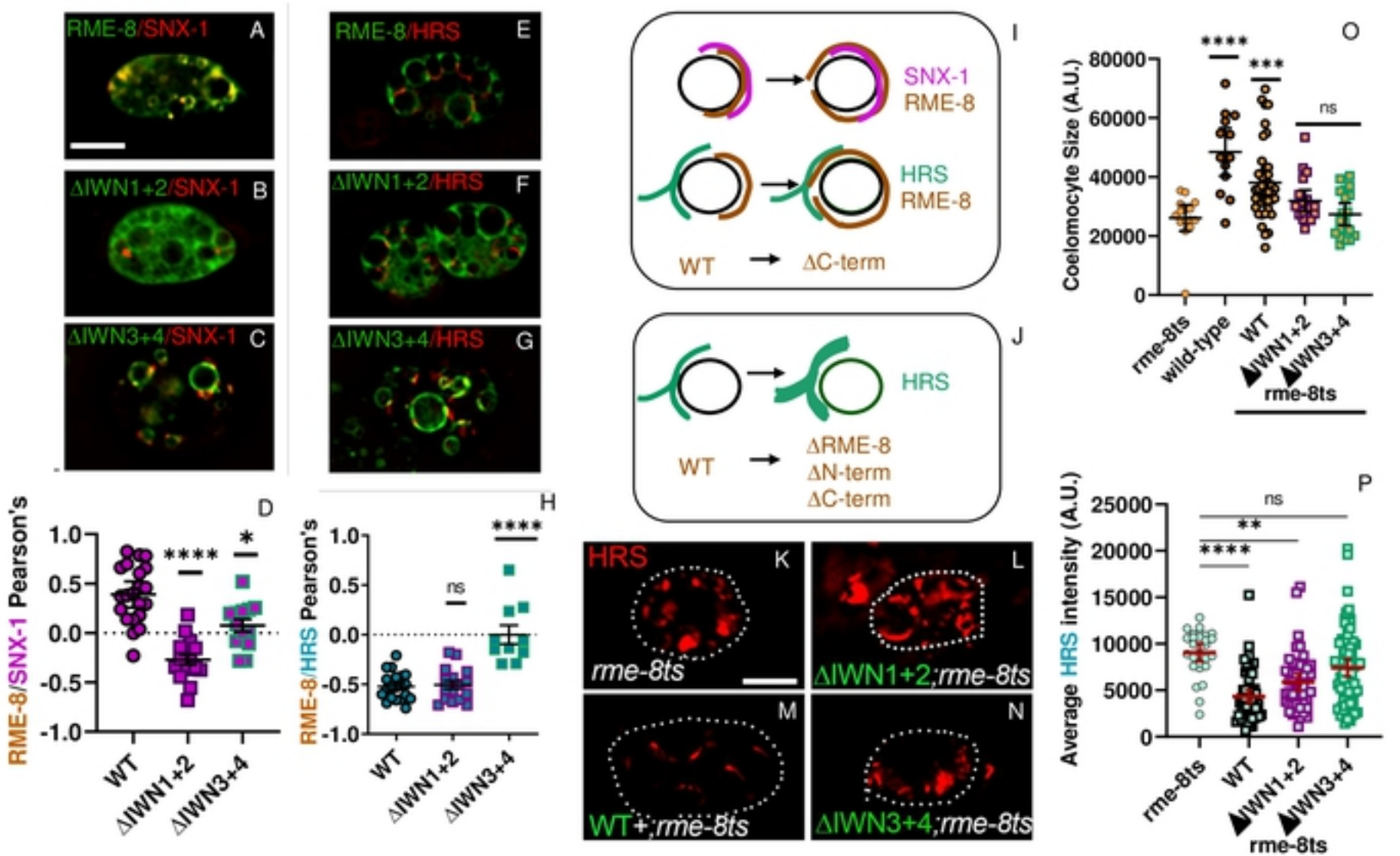
RME-8/SNX-1
A
ΔIWN1+2/SNX-1
B
ΔIWN3+4/SNX-1
C
RME-8/HRS
E
ΔIWN1+2/HRS
F
ΔIWN3+4/HRS
G
RME-8/SNX-1 Pearson's
D
WT
ΔIWN1+2
ΔIWN3+4
RME-8/HRS Pearson's
H
ns
I
SNX-1
RME-8
HRS
RME-8
WT
ΔC-term
J
HRS
WT
ΔRME-8
ΔN-term
ΔC-term
HRS
K
rme-8ts
L
ΔIWN1+2;rme-8ts
M
WT+;rme-8ts
N
ΔIWN3+4;rme-8ts
O
Coelomocyte Size (A.U.)
rme-8ts
wild-type
WT
ΔIWN1+2
ΔIWN3+4
rme-8ts
P
Average HRS intensity (A.U.)
rme-8ts
WT
ΔIWN1+2
ΔIWN3+4
rme-8ts

Figure 3. RME-8 C-terminal regions mediate its recycling versus degradative domain segregation. Both N-terminal and C-terminal regions are important for HRS (HGRS-1) uncoating activity. (A-C) Micrograph of pCUP-4::GFP::RME-8 wild-type, N-terminal, and C-terminal truncations co-expressed with tagRFP::SNX-1 in coelomocytes of wild-type animals. (D) Quantification of colocalization of pCUP-4::GFP::RME-8 wild-type and truncations with tagRFP::SNX-1 in coelomocytes of wild-type animals. (E-G) Micrograph of pCUP-4::GFP::RME-8 wild-type, N-terminal, and C-terminal truncations co-expressed with tagRFP::HRS (HGRS-1) in coelomocytes of wild-type animals. (H) Quantification of colocalization of GFP::RME-8 wild-type and truncations with tagRFP::SNX-1 in wild-type animals. (I) Illustration of the microdomain segregation that is disrupted when IWN3 and IWN4 regions are deleted in RME-8. (J)) Illustration of the accumulation of HRS (HGRS-1) that occurs in the absence of RME-8, and N-terminal and C-terminal deletions. (O) Quantification of coelomocyte size in rme-8ts mutant animals expressing ectopic RME-8+, N-terminal, or C-terminal truncations. (P) Quantification of tagRFP-HRS/HGRS-1 average intensity in rme-8ts animals expressing pCUP-4::GFP::RME-8+, N-terminal, or C-terminal truncations. Each data point is an individual worm, error bars indicate Mean with 95% CI, ANOVA statistical analysis done in Prism with $p<0.5$=*, $p<0.01$=**, $p<0.001$=***, $p<0.0001$=****. Scale bars are 5 microns in whole coelomocyte images.

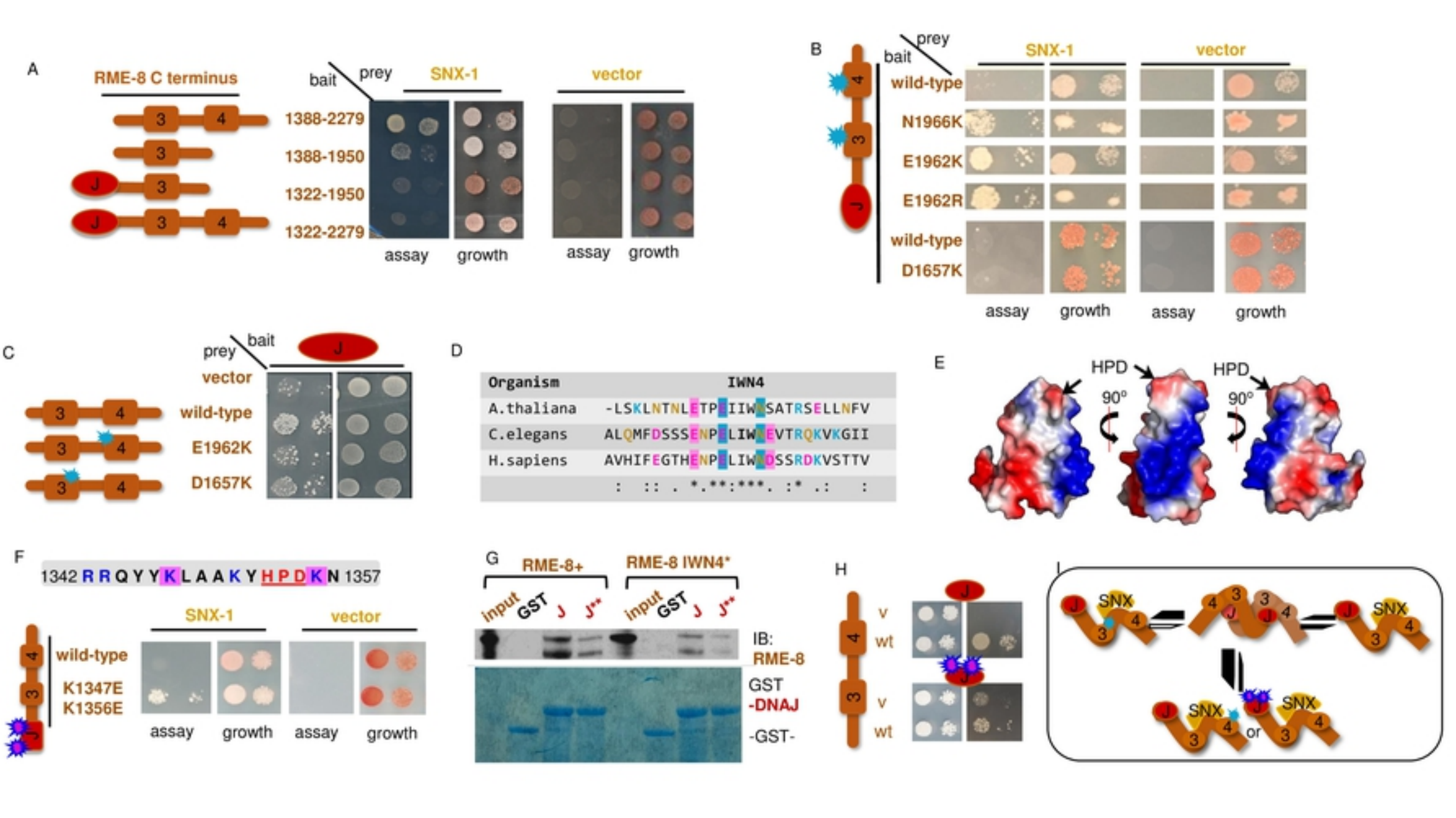
A
RME-8 C terminus
3
4
J
bait
prey
SNX-1
vector
1388-2279
1388-1950
1322-1950
1322-2279
assay
growth
B
wild-type
N1966K
E1962K
E1962R
D1657K
C
E1962K
D1657K
D
Organism
IWN4
A.thaliana
C.elegans
H.sapiens
E
HPD
90°
F
1342 R R Q Y Y K L A A K Y H P D K N 1357
K1347E
K1356E
G
RME-8+
RME-8 IWN4*
input
GST
IB:
RME-8
GST
-DNAJ
-GST-
H
v
wt
I
SNX
or

Figure 4. The RME-8 DNAJ , IWN4, and IWN3 domains mediate SNX-1 and RME-8 self-interactions. (A) SNX-1 (aa221-472) expressed in pDEST22™ tested for interaction with empty vector or fragments of the RME-8 C-terminus expressed in pDEST32™ using JDY27 containing URA3, ADE2, and HIS3 reporter genes. 5ul of suspended yeast at 1, and 0. 1 OD's s were spotted on SC-LEU-TRP growth or SC-LEU-TRP-URA assay media. A schematic representation of the RME-8 fragments tested are illustrated to the left of the yeast two hybrid assay. (B) PCR mutagenesis of the RME-8 (DNAJ-end) fragment yielded two mutants in IWN4. Both mutations were lysine substitutions at Glutamic Acid 1955 and Asparagine 1966, that enabled an RME-8(C-term)/SNX-1(BAR) growth on the stringent assay media SC-LEU-TRP-URA. An arginine substitution at position 1962 did not enabled growth on the stringent assay media SC-LEU-URA. A schematic of the RME-8 fragment is illustrated to the left of the assay. 5ul of suspended yeast at 0.5 and 0.05 OD's s were spotted on SC-LEU-TRP growth or SC-LEU-TRP (-URA or +20mM 3AT) assay media. (C) Fragments of RME-8 C-terminus (no DNAJ) in the Duplex LexA™ 2-micron yeast two hybrid system were tested for their ability to interact with the DNAJ domain (1322-1388). 5ul of suspended yeast at 2, 0.2, and 0.02 OD's s were spotted on SC-HIS-URA-TRP growth or SC GAL-HIS-TRP-LEU SC assay media. IWN3 and IWN4 mutants of the C-terminus displayed diminished interaction compared to wild-type. The isolated IWN4 fragment displayed similar growth to full length. A schematic of the mutants and fragments are illustrated to the left of the assay. (D) alignment of IWN4 from C. elegans, H. sapiens and A. thaliana. RME-8 E1962 and N1966 found in the screen are highlighted with blue. Additional acidic residues are highlighted in pink. (E) Three views of an electrostatic representation of the RME-8 DNAJ domain threaded onto PDB file 2OCH. Blue indicates basic, and red indicates acidic surfaces. The HPD catalytic triad of DNAJ domains is indicated by arrows. The center image displays the basic nature of helix II of the DNAJ domain. (F) Lysines and Arginines of helix II were targeted for doped oligo mutagenesis and selected for increased interaction with SNX-1. The two lysines identified by the screen are highlighted in pink. The red underline indicates residues that were identified by Ahmad et al 2011 to be defective in DNAJ/DNAK(Hsc70) interactions. The aa1322-2279 fragment with lysines at position 1347 and 1356 substituted with glutamic acid was sufficient to show growth on assay media when combined with SNX-1 BAR domain. A schematic of the Fragment mutated represented to the left of the assay. 5ul of suspended yeast at 1, and 0.1 OD's were spotted on SC-LEU-TRP growth or SC-LEU-TRP-URA assay media. (G) Fragments of HA-tagged RME-8 C-terminus (no DNAJ) wild-type and IWN4* expressed in an in vitro TnT™ system were incubated with DNAJ-GST or DNAJ*(K1347E/K1356E)-GST Sepharose beads. The bound fraction was run on an SDS-PAGE gel and probed with an HA-antibody. The incubation reaction was also run on a separate gel and stained with Coomassie Blue to indicate the amount of GST-tagged DNAJ domain. DNAJ** disrupted the RME-8/DNAJ interaction. (H). The aa1322-1388 (DNAJ) fragment with lysines at position 1347 and 1356 substituted with glutamic acid disrupted the RME-8/DNAJ interaction. A schematic of the Fragment mutated represented to the left of the assay. 5ul of suspended yeast at 1, and 0.1 OD's were spotted on SC-LEU-TRP growth or SC-LEU-TRP-URA assay media. (I) An illustration of our hypothesis that mutations in DNAJ, IWN4, and IWN3 disrupt RME-8 self-interaction.

Figure S4. Supplement to Figure 5. Empty vector or SNX-1 (aa221-472) expressed in pDEST22™ tested for interaction with of the RME-8 C-terminus with our without its DNAJ domain, and mutants isolated in the screen. The RME-8 fragments were expressed in pDEST32™ using JDY27 containing URA3, ADE2, and HIS3 reporter genes. 5ul of suspended yeast at 1, and 0.1 OD's were spotted on SC-LEU-TRP growth, or assay plates with increasing stringency; SC-LEU-TRP-HIS, SC-LEU-TRP-HIS+25mM 3AT, and SC-LEU-TRP-URA. A schematic representation of the RME-8 fragments tested are illustrated to the left of the yeast two hybrid assay.

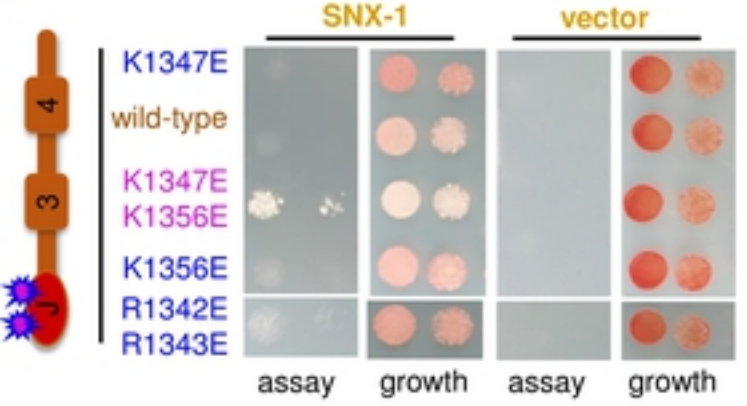

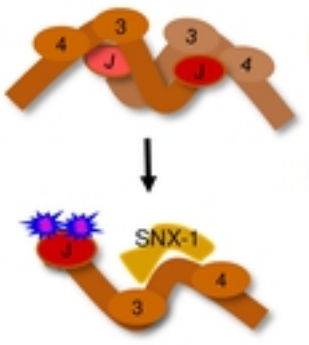

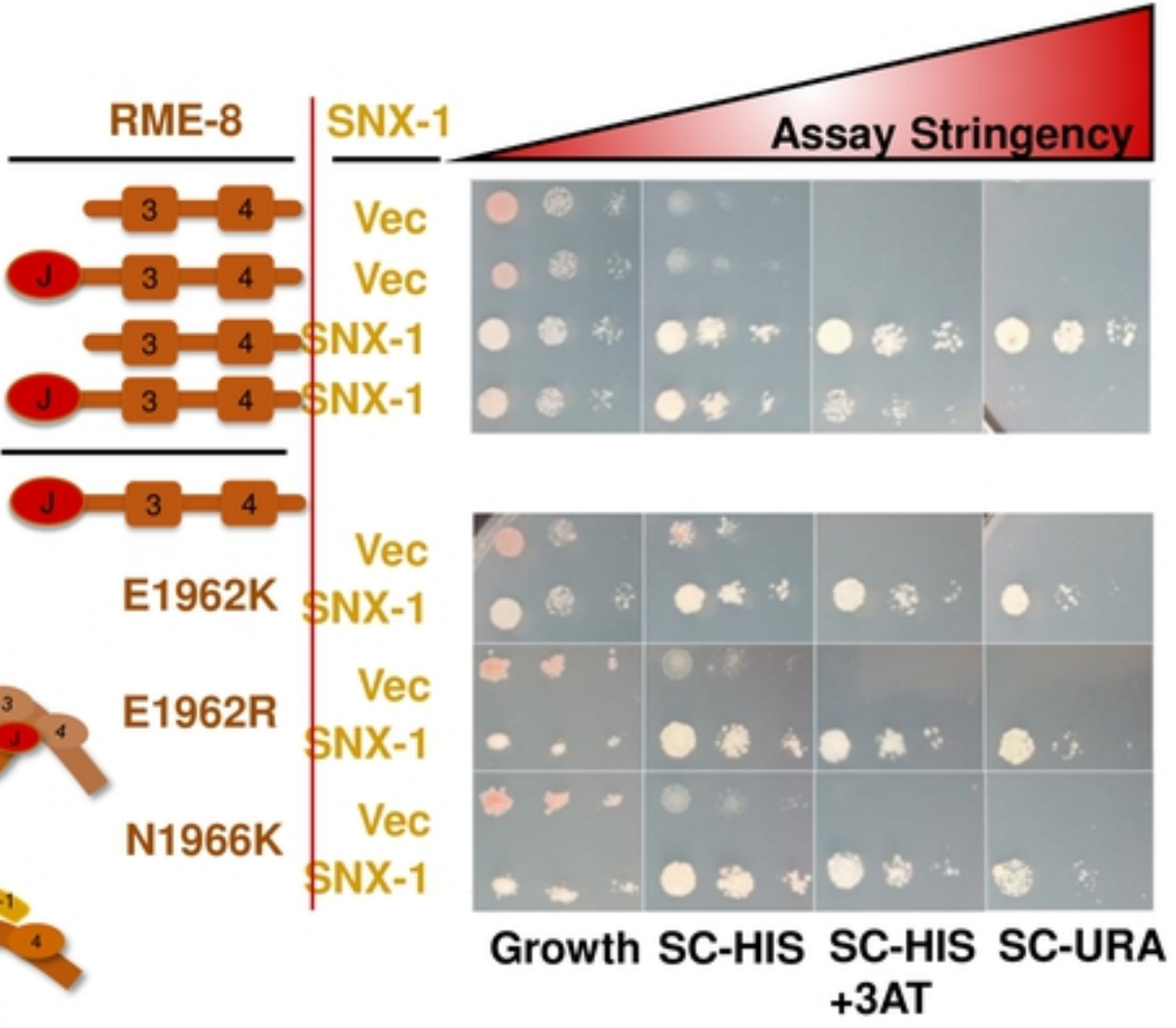

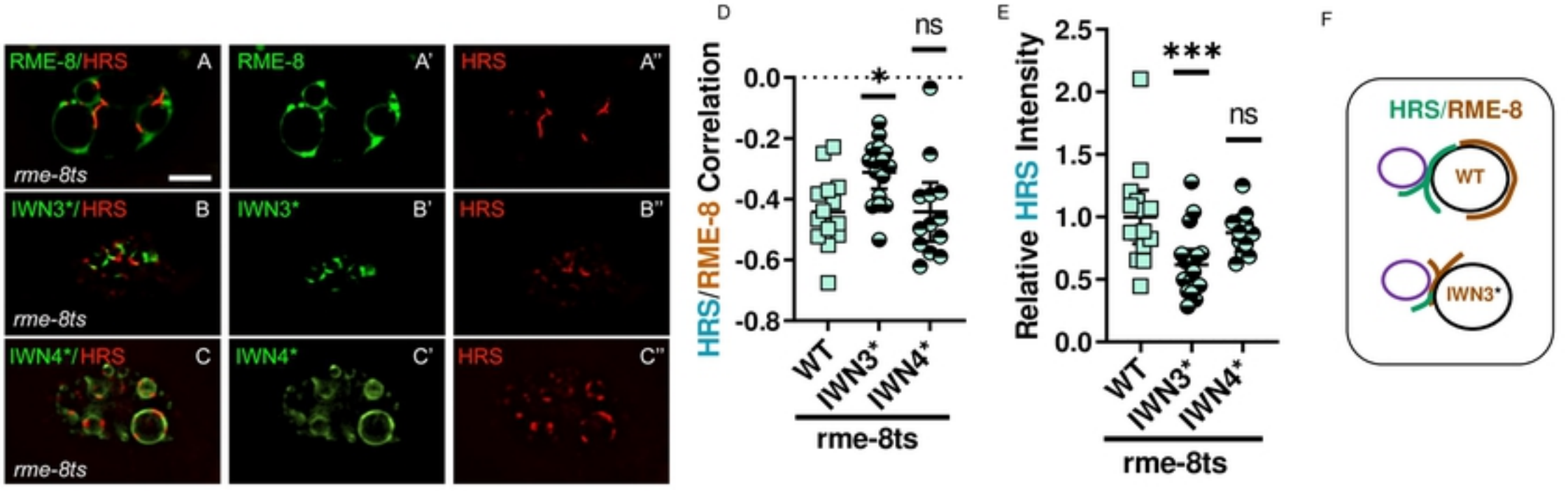

Figure 5. IWN3* mutant alters both RME-8/HRS colocalization and HRS accumulation. (A-A'') Micrograph of pCUP-4::GFP::RME-8 co-expressed with tagRFP::HRS(HGRS-1) in coelomocytes of rme-8(b1023ts) animals. Single channels and the merge are displayed. (B-B''') Micrograph of pCUP-4::GFP::RME-8 D1657K mutation in IWN3 (IWN3*) co-expressed with tagRFP::HRS(HGRS-1) in coelomocytes of rme-8ts animals. Single channels and the merge are displayed. (C-C'') Micrograph of pSNX-1::tagRFP::HRS(HGRS-1) co-expressed with RME-8 IWN4 triple glutamic acid to lysine substitution at positions 1959,1961, and 1966 (IWN4*) in rme-8ts mutant animals. Single channels and the merge are displayed (D) Quantification of colocalization of HRS(HGRS-1) with RME-8 WT, IWN3* and IWN4*. (E) Quantification of tagRFP::HRS/HGRS-1 average intensity rme-8ts mutant animals expressing RME-8 WT, IWN3* and IWN4*. (F) Illustration of the interior shift and increased HRS overlap of the RME-8 microdomain that occurs upon the introduction of D1657K in IWN3 (indicated in brown). Illustration of the shrinkage of the HRS(HGRS-1) microdomain upon the introduction of D1657K in IWN3 (indicated in green). Each data point is an individual worm, error bars indicate Mean with 95% CI, ANOVA statistical analysis done in Prism with $p<0.5$=*, $p<0.01$=**, $p<0.001$=***, $p<0.0001$=****. Scale bars are 5 microns in whole coelomocyte images.

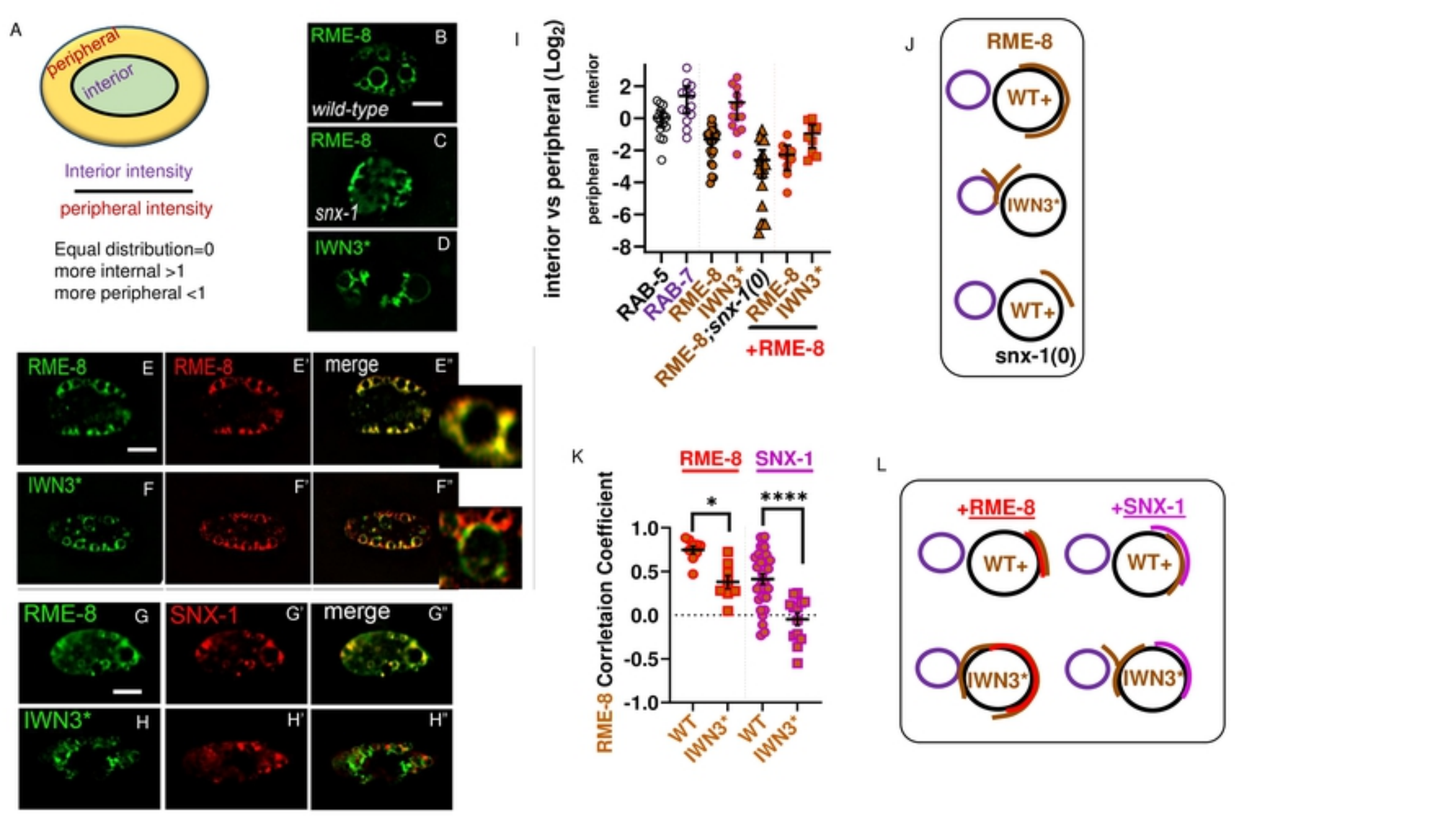
A
peripheral
interior
Interior intensity
peripheral intensity
Equal distribution=0
more internal >1
more peripheral <1
RME-8 B
wild-type
RME-8 C
snx-1
IWN3* D
I
interior vs peripheral (Log2)
interior
peripheral
2
0
-2
-4
-6
-8
RAB-5
RAB-7
RME-8
IWN3*
RME-8;snx-1(0)
RME-8
IWN3*
+RME-8
J
RME-8
WT+
IWN3*
WT+
snx-1(0)
RME-8 E
RME-8 E'
merge E"
IWN3* F
F'
F"
RME-8 G
SNX-1 G'
merge G"
IWN3* H
H'
H"
K
RME-8
SNX-1
*
****
RME-8 Corrletaion Coefficient
1.0
0.5
0.0
-0.5
-1.0
WT
IWN3*
WT
IWN3*
L
+RME-8
+SNX-1
WT+
WT+
IWN3*
IWN3*

Figure 6. SNX-1, IWN3* and RME-8 expression levels control RME-8 microdomain localization and positioning. (A) Micrograph of pCUP-4::GFP::RME-8 wild-type animals. (B) Micrograph of pCUP-4::GFP::RME-8 snx-1(0) mutant animals. (C) Micrograph of pCUP-4::GFP::RME-8 D1657K (IWN3*) in wild-type animals. (D-D'') Micrograph of GFP::RME-8 co-expressed with tagRFP::RME-8 in coelomocytes. Single channels and the merge are displayed, with an inset of an endosome from the merged channels. (E-E'') Micrograph of GFP::RME-8 co-expressed with tagRFP::RME-8 in coelomocytes. Single channels and the merge are displayed, with an inset of an endosome from the merged channels. (F-F'') Micrograph of GFP::RME-8 D1657K mutation in IWN3 (IWN3*) co-expressed with tagRFP::RME-8 in coelomocytes. Single channels and the merge are displayed with an inset of an endosome from the merged channels. (G-G'') Micrograph of GFP::RME-8 co-expressed with tagRFP::SNX-1 in coelomocytes. Single channels and the merge are displayed with an inset of an endosome from the merged channels. (H-H'') Micrograph of GFP::RME-8 D1657K mutation in IWN3 (IWN3*) co-expressed with tagRFP::SNX-1 in coelomocytes. Single channels and the merge are displayed with an inset of an endosome from the merged channels. (I) Ratio of intensity of interior versus peripheral endosome labeling of RAB-5, RAB-7 (from figure 2B and 2C) and the indicated GFP::RME-8 allele from B-F'' plotted on a Log2 scale. A value of 0.0 indicates intensity is equal between the peripheral and interior regions. A two-fold increase in interior intensity would give a value of 1.0 and a two-fold decrease would give a value of -1.0. See illustration in A. (J) Illustration of the interior shift of the RME-8 microdomain that occurs upon the introduction of D1657K in IWN3 (indicated in brown). (K) Quantification of colocalization of tagRFP::RME-8 (From D-E'') or tagRFP::SNX-1 (from F-G'') with GFP::RME-8 WT, IWN3* and IWN4*. (L) Illustration of the peripheral or interior shift of a wild-type RME-8 microdomain (indicated in red) that occurs upon coexpression with GFP::RME-8(+) or GFP::RME-8 D1657K (IWN3*), (all indicated in brown). Illustration of the tagRFP::SNX-1 (indicated in magenta) colocalization that occurs upon coexpression with the introduction of GFP::RME-8(+), GFP::RME-8 D1657K (IWN3*) (all indicated in brown).

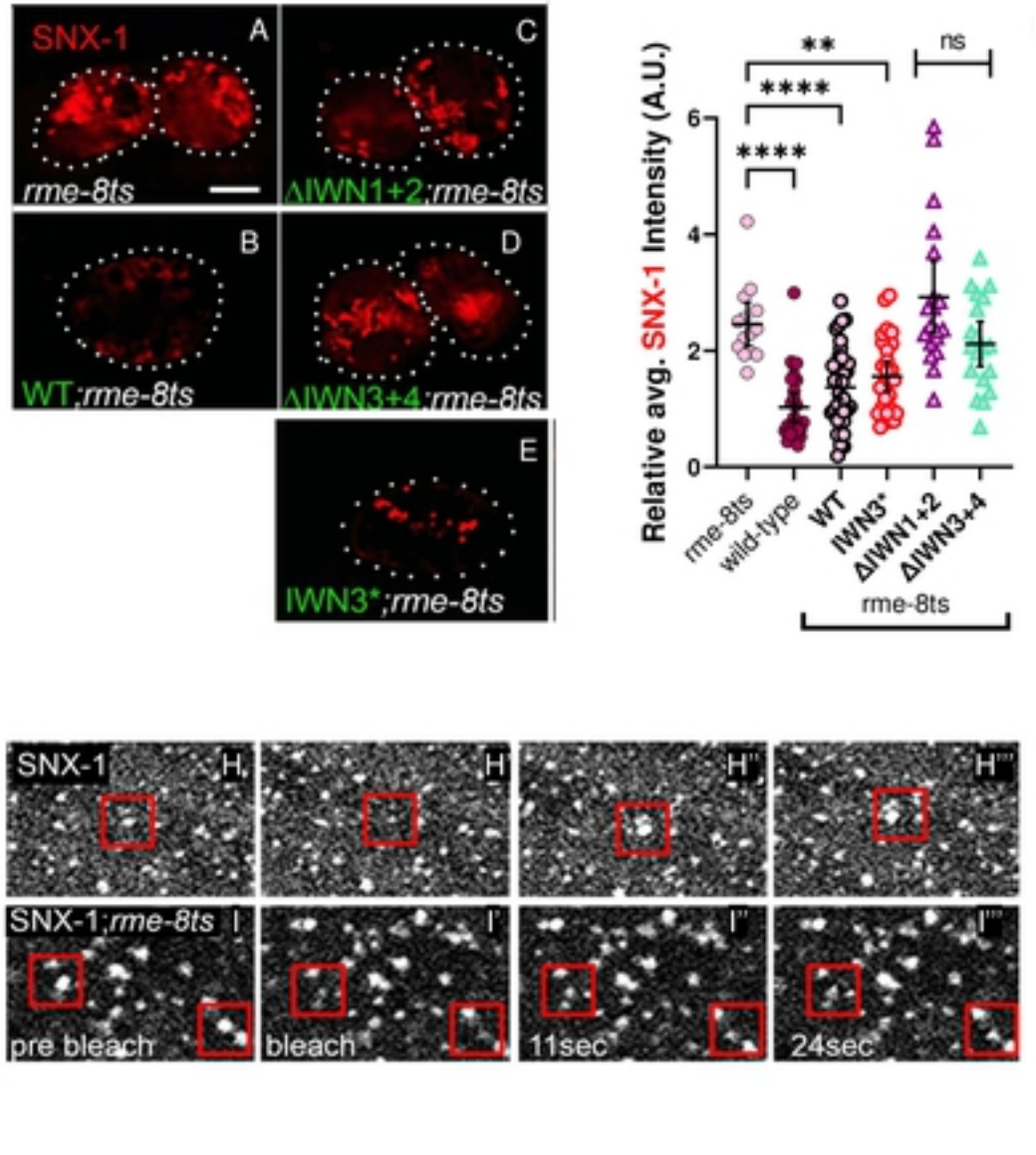

Figure 7. SNX-1 is a target of RME-8 activity. (A-E) Micrograph of tagRFP::SNX-1 co-expressed with GFP::RME-8 WT, N-terminal and C-termainal truncations, as well as the IWN3* point mutant in rme-8ts animals. (F) Quantification of tagRFP::SNX-1 average intensity displayed in A-H. (G) Quantification of the fiber length tagRFP::SNX-1 microdomains in animals expressing GFP::RME-8, no RME-8 and GFP::IWN4* in rme-8ts mutant animals. (H-I''') FRAP analysis of GFP-SNX-1 positive endosomes expressed in the hypodermis of wild-type and rme-8ts animals. Red squares indicate endosomes that were bleached. (J) Quantification of FRAP analysis of GFP-SNX-1 positive endosomes expressed in the hypodermis of wild-type and rme-8ts animals. $p<0.0001$. ANOVA statistical analysis done in Prism, $p<0.5$=*, $p<0.01$=**, $p<0.001$=***, $p<0.0001$=****. Scale bars are 5 microns in whole coelomocyte and hypodermis subcellular images.

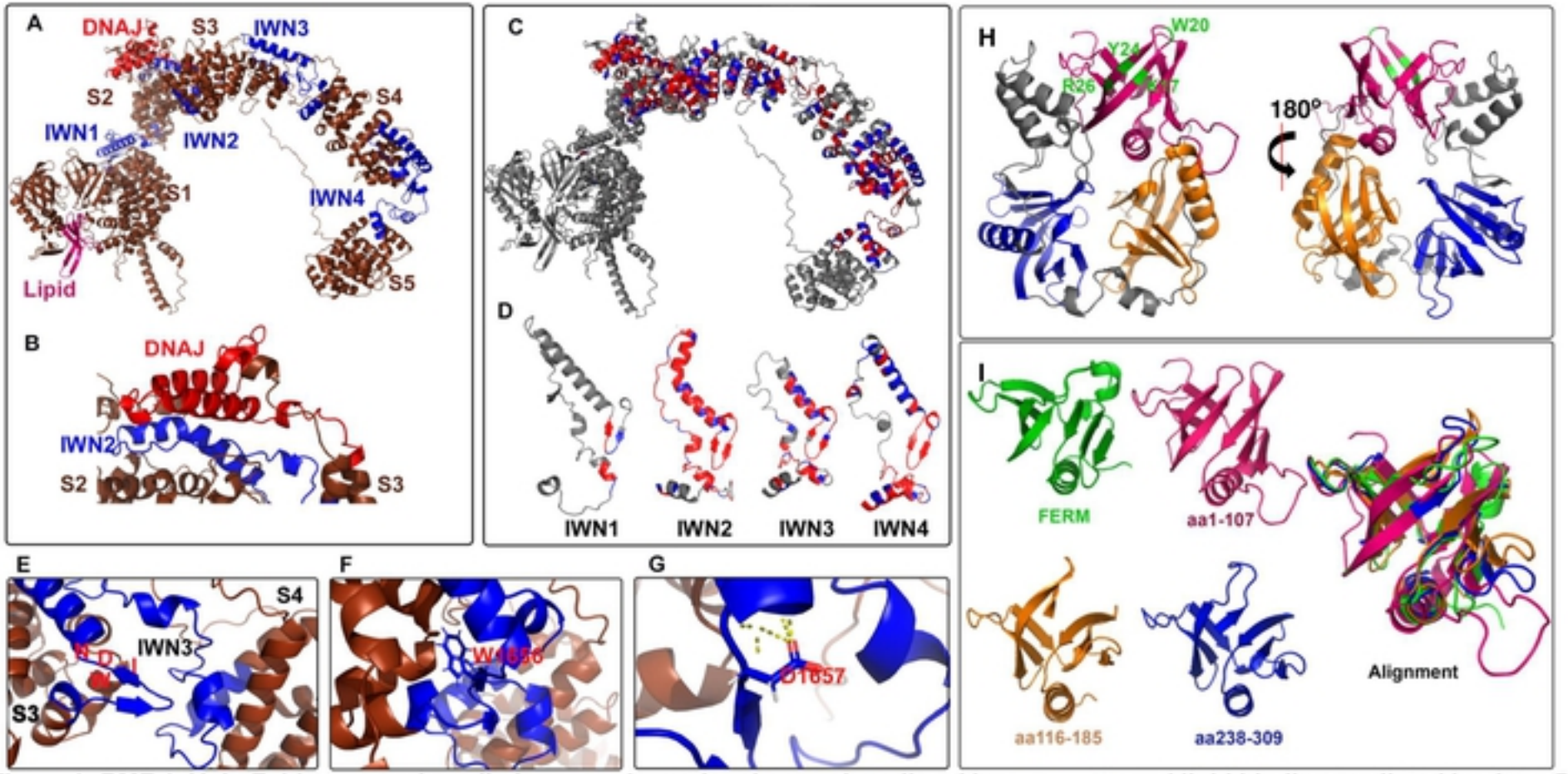

Figure 8. RME-8 AlphaFold structural predictions: conformational control mediated by IWN motifs and lipid binding mediated by three PH-like domains. (A) Ribbon diagram of AlphaFold generated PDB file. The previously defined lipid binding domain is depicted in magenta. IWN domains defined by Zhang et al 2001 are depicted in blue. The DNAJ domain is depicted in red. The five alpha-solenoid regions are labeled S1-S5. (B) A zoomed in view of the juxtaposition of IWN2 and the DNAJ domain, with portions of alpha-solenoid 2 and alpha-solenoid 3 that are separated by the IWN2 elbow-like structure. (C) ribbon diagram demonstrating the conserved residues from Figure 1 and Figure S1. Highly conserved residues are colored in red, moderately conserved residues are colored in blue. (D) Using the same color scheme as panel C, the IWN domains are represented to show their similarity in form as well as conservation across Eukarya. (E) A zoomed in view of the IWN3 linker between alpha-solenoid 3 and alpha solenoid 4. The position of the (I) Isoleucine, (W)Tryptophan, (D) Aspartic acid, and (N) Asparagine of the IWN3 domain are indicated in red. (F) The position of W1656 of the IWN3 domain is predicted to be buried, and on the opposite face of the Beta-strand as I, D and N. (G) The position of D1656 which is mutated to lysine in IWN3* in the predicted structure. (H) Ribbon diagram of the first 400 amino acids of the AlphaFold generated structure. The previously defined domain is indicated in magenta, with key residues for phospholipid binding indicated in green. The two additional PH-like domains are indicated in blue and orange. (I) Ribbon diagrams of the FERM domains used to align to the three beta-strand rich regions of the N-terminus in green. The three PH-like domains of the RME-8 N-terminus are colored as in (H). An alignment of all four Beta-strand rich regions is shown to the right of the individual

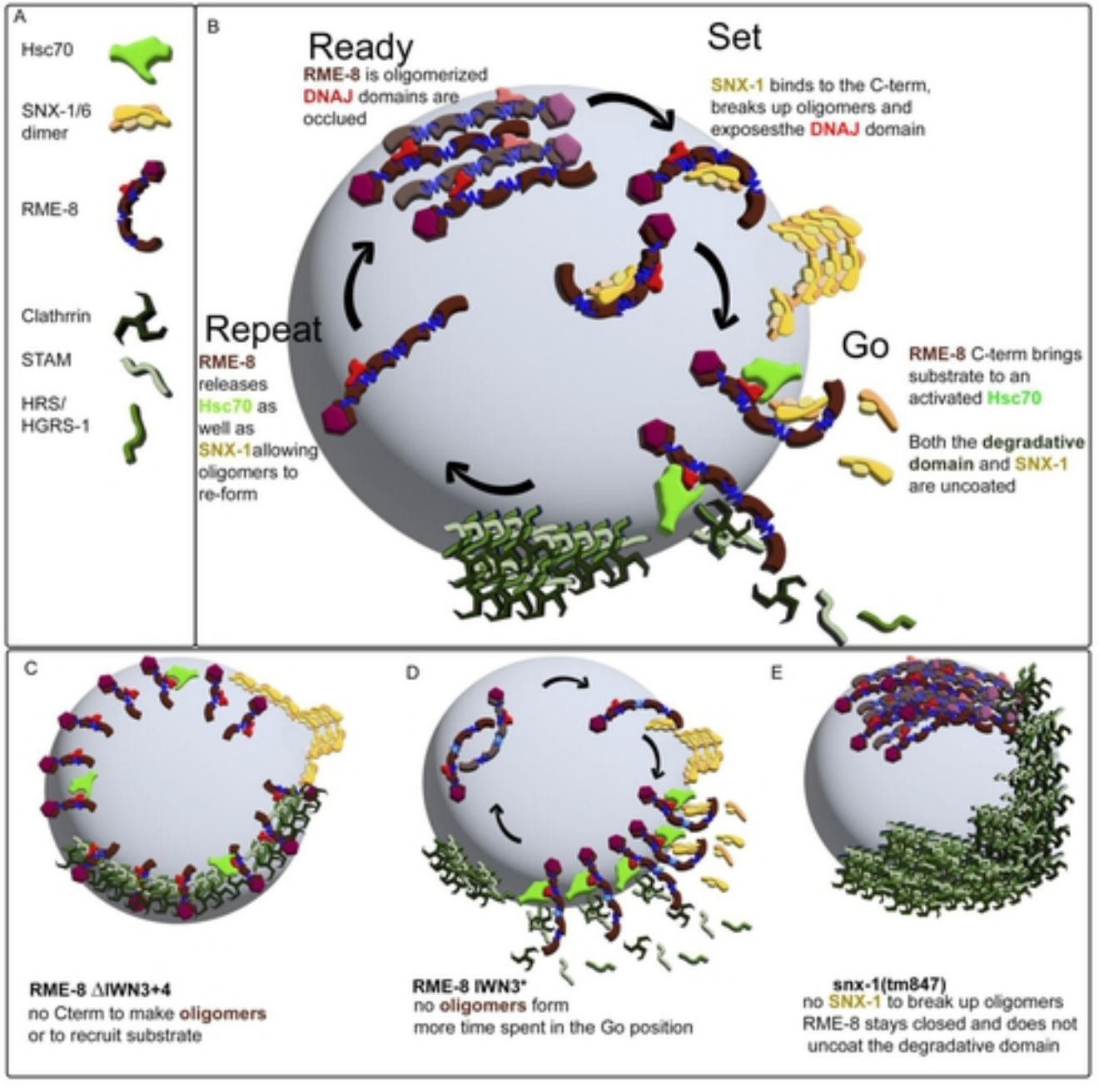

Figure 9. Ready Set Go model for cyclical activation of RME-8. (A) Legend (B) Illustration of the Ready Set Go Repeat model of cyclical RME-8 activation on the endosome. We propose that RME-8 exists in a few different states in the cell; an oligomerized inactive form with the DNAJ domain occluded (Ready), an open form bound to SNX-1 with the DNAJ domain exposed (Set). An active form bound by Hsc70 and substrate (Go). This model is informed by the idea that the RME-8 activator SNX-1 is also a target of RME-8 uncoating activity, allowing the process to be cyclical. (C) An illustration of the spread of RME-8 and accumulation of SNX-1 and HRS/HGRS-1 in coelomcytes expressing RME-8 C-terminal truncations. (D) An illustration of the model for how the IWN3* mutant disrupts RME-8 oligomers independently of SNX-1 allowing for more RME-8 to be in the active "go" state. (E) Illustration of the proposed HRS/HGRS-1 and RME-8 oligomeric accumulation that occurs in snx-1(0) animals as observed in previous studies [10].

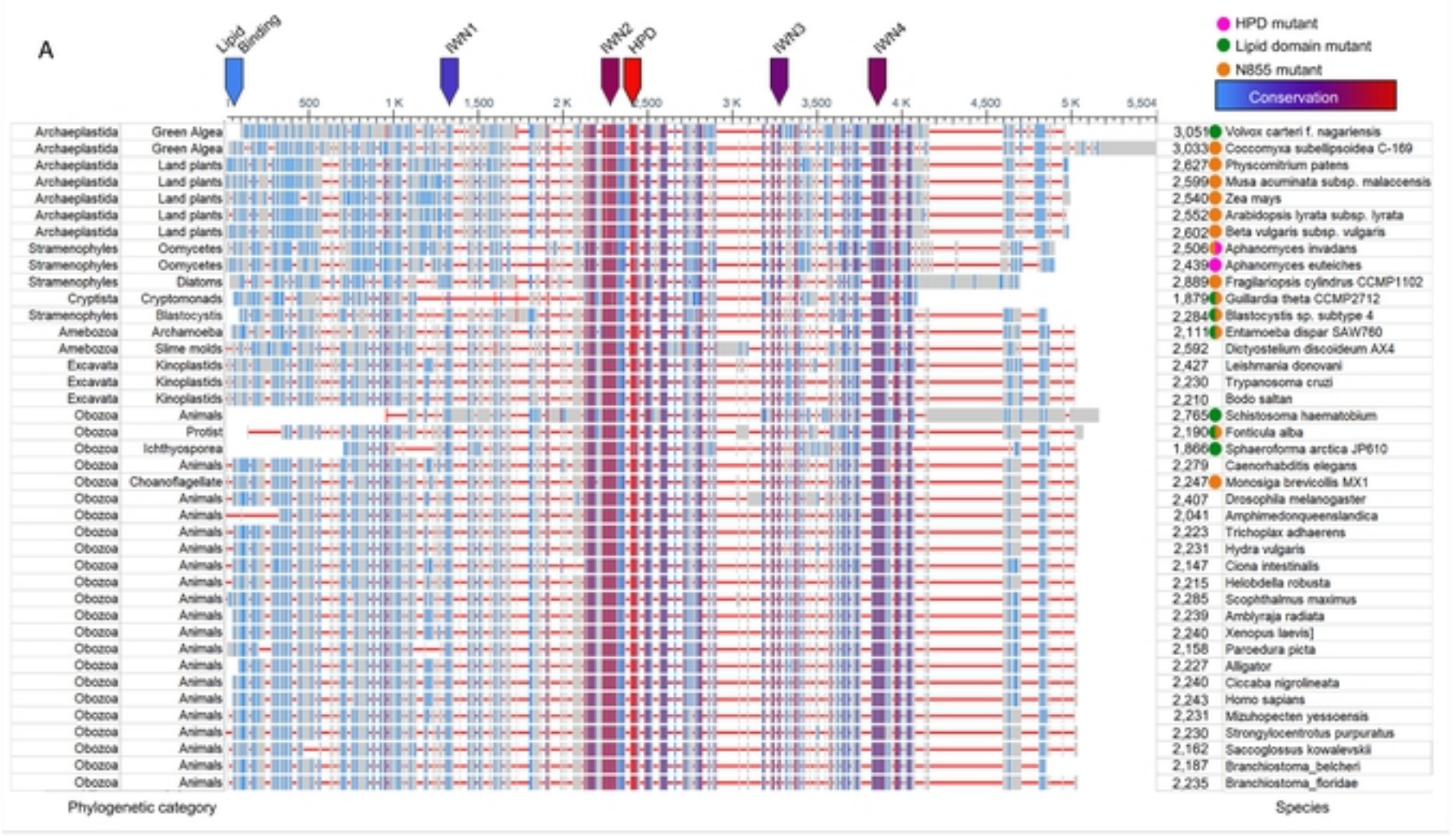

Figure S1 supplement to figure 1. (A) Expansion of figure 1C with more organisms included. (B) Annotated display of C. elegans RME-8 sequence from the multiple sequence alignment in Figure 1B. The defined lipid binding domain from [6] is indicated in cerulean. The predicted expanded lipid binding domain from this study is indicated in magenta. IWN repeats defined by [2] are highlighted in green. The DNAJ domain is highlighted in grey. Yellow arrows indicate regions of high conservation that lie outside of established functional domains. Individual amino acids are colored according to conservation across Eukarya with grey indicating no conservation, blue indicating moderate conservation and red indicating high conservation.


B
Lipid binding
Predicted lipid binding domain expansion
IWN1
IWN2
DNAJ
IWN3
IWN4

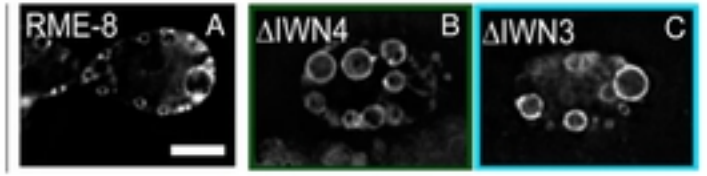

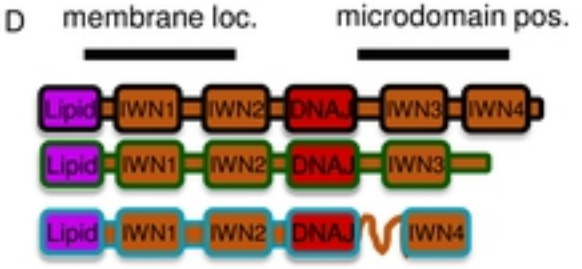

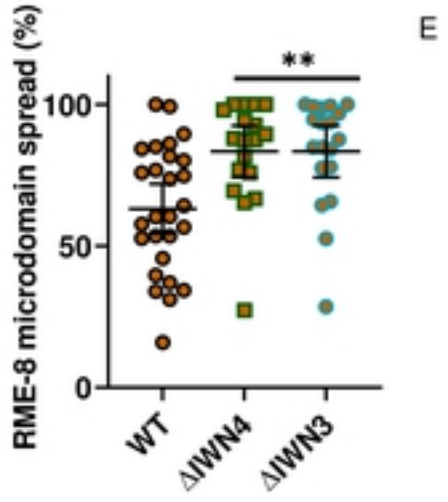

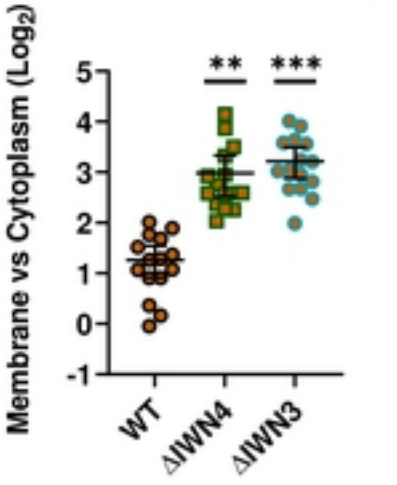

Figure S2 supplement to figure 2. (A-C) Micrograph of pSNX-1::GFP::RME-8 full length, ΔIWN3 and ΔIWN4 truncations, expressed in wild-type animals. (D) Illustration of wild-type, ΔIWN3 and ΔIWN4 truncations of RME-8. (E) Quantification of the percentage of an endosome covered by the indicated GFP-RME-8 wild-type and truncation mutants. (F) Ratio of the GFP::RME-8 intensity in the cytoplasm versus on the membrane in the indicated GFP::RME-8 wild-type and truncations. The values are also plotted on a Log2 scale. All micrographs are deconvolved widefield images (see methods). In I-K each data point is an individual worm, error bars indicate Mean with 95% CI, ANOVA statistical analysis done in Prism with p<.5=*, p<.01=**, p<.001=***, p<.0001=****. Scale bars are 5 microns in whole coelomocyte images.

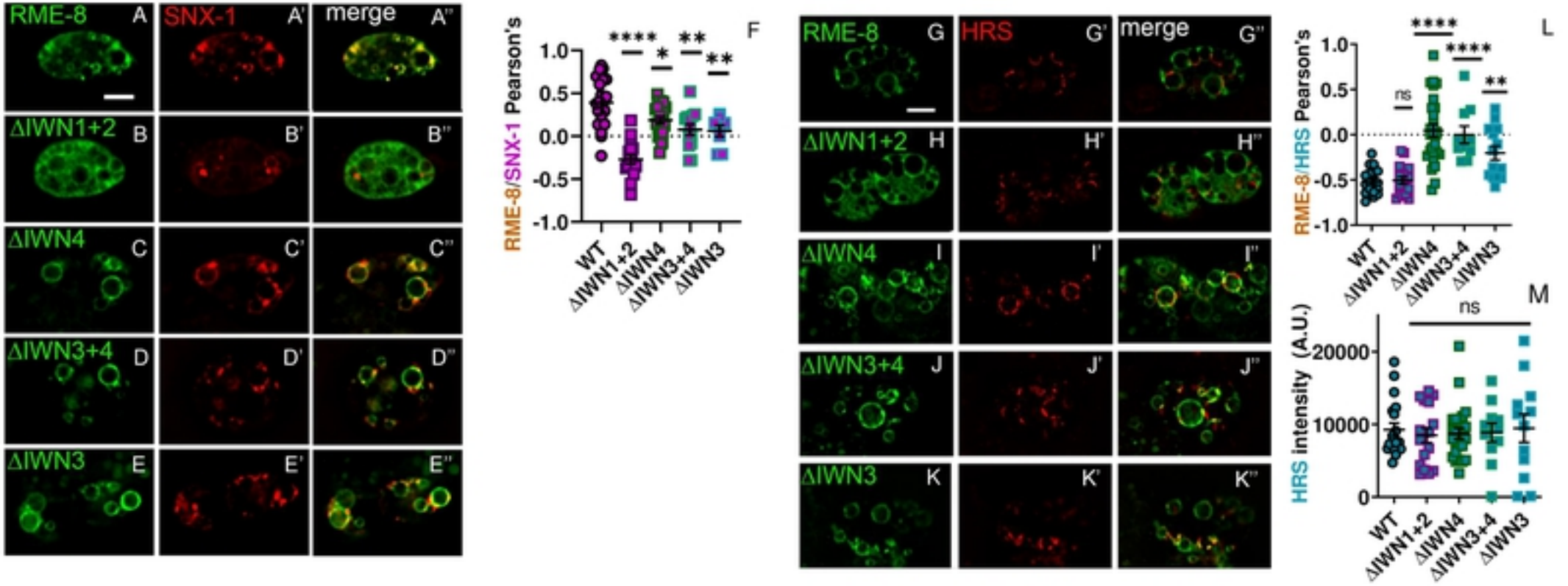

Figure S3 supplement to figure 3. (A-E") Micrograph of pCUP-4::GFP::RME-8 wild-type, N-terminal, and C-terminal truncations co-expressed with tagRFP::SNX-1 in coelomocytes of wild-type animals. (F) Quantification of colocalization of pCUP-4::GFP::RME-8 wild-type and truncations with tagRFP::SNX-1 in coelomocytes of wild-

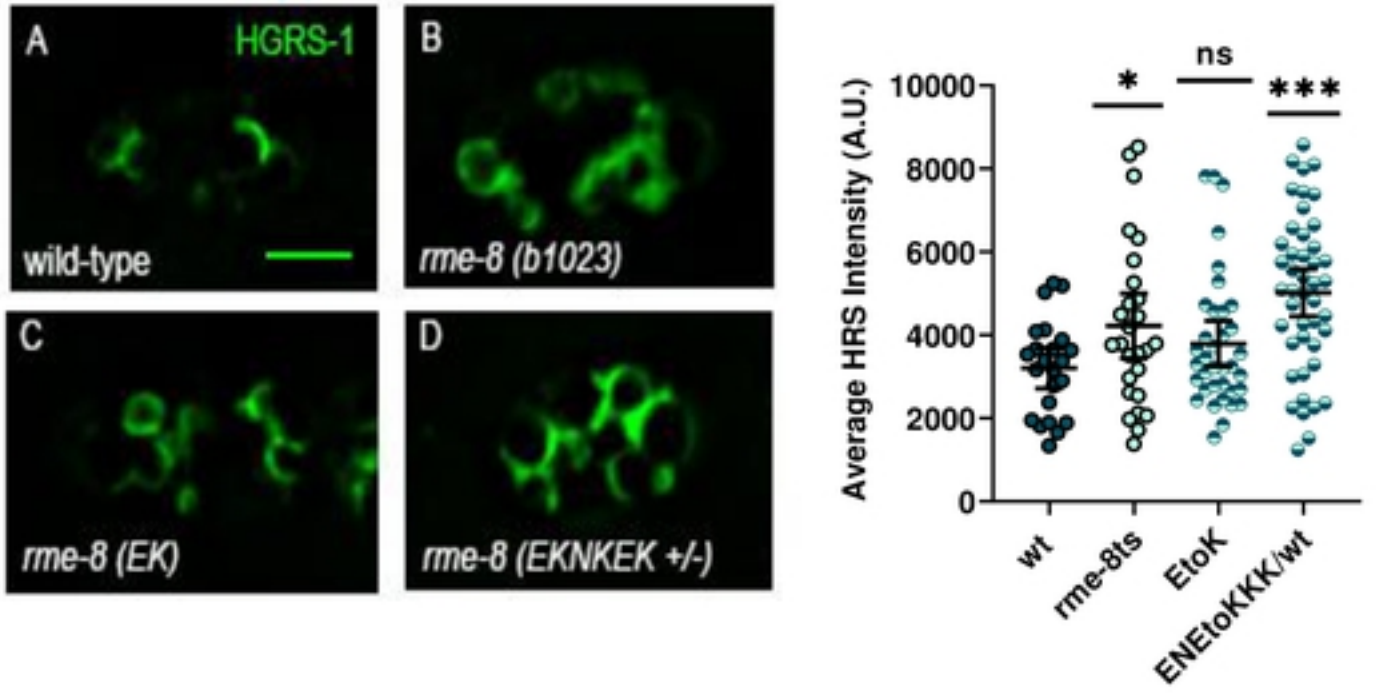

Figure S4. Supplement to figure 5. IWN4 mutants are defective in removing HRS/HGRS-1. (A-D) Micrograph of pSNX-1::Citrine::HRS/HGRS-1 expressed in coelomocytes of wild-type (A) rme-8ts(b1023) animals (B), CRISPR generated rme-8 E1962K animals (C), and heterozygous CRISPR generated rme-8 (E1962K/N1966K/E1967K) animals(D). **(E)** Quantification HRS/HGRS-1 average intensity animals represented in A-D. Each data point is an individual worm, error bars indicate Mean with 95% CI, ANOVA statistical analysis done in Prism with p<.5=*, p<.01=**, p<.001=***, p<.0001=****. Scale bars are 5 microns in whole coelomocyte images.